DEMONSTRATION OF A CLOSED LOOP DIGITALLY ENABLED MANUFACTURING PROCESS USING ADVANCED METROLOGY TECHNIQUES

by

Michael Erickson

A thesis submitted to the faculty of
The University of North Carolina at Charlotte
in partial fulfillment of the requirements
for the degree of Master of Science in
Mechanical Engineering

Charlotte

2018

Approved by:

_____
Dr. John Ziegert

_____
Dr. Edward Morse

_____
Dr. Tony Schmitz

ABSTRACT

MICHAEL ERICKSON. Demonstration of a closed loop digitally enabled manufacturing process using advanced metrology techniques. (Under the direction of DR. JOHN ZIEGERT)

This thesis details the use of advanced coordinate metrology techniques to digitally enable manufacturing through the demonstration of predictive shimming in the assembly of a power plant generator Frame and Stator Core. A process was developed to create digital models of the as-built generator components, calculate the desired gap dimensions, and pre-manufacture shims to maintain these gaps. The research illustrates a potential to reduce cost, improve product quality, and increase productivity in large scale manufacturing.

The geometric features of the components were measured with a laser tracker and analyzed in metrology software to perform digital assembly. Shim comparisons were made between those that were actually used in the generator assembly and those that were predicted digitally. After performing an experiment and finite element analysis to evaluate a generator Frame, it was found that the component's shape was largely affected by its support condition and gravitational sag. Mitigation strategies were suggested to force the Frame into its desired shape during measurement.

In total, six generator assemblies were measured and two assembly tests using pre-manufactured shims were conducted. Each test successfully produced in-tolerance alignments and demonstrated the benefits and feasibility of the digitally enabled process. Basic metrics were used to evaluate the quality and repeatability of the project's measurements and it was found that the activities in the surrounding shop environment affected the measurement quality.

DEDICATION

I would like to dedicate this work to all of my family for their endless support and my Lord and Savior Jesus Christ in whom I find my strength.

ACKNOWLEDGEMENTS

I thank my advisors Dr. John Ziegert and Dr. Edward Morse for their guidance and direction in the success of my thesis. I also thank Dr. Tony Schmitz for serving as part of my committee. I thank my project partner and good friend, Corbin Grohol, who contributed as much as I to the success of the project.

TABLE OF CONTENTS

LIST OF TABLES

LIST OF FIGURES

CHAPTER 1. INTRODUCTION

Manufacturing traditionally utilizes metrology for quality purposes related to inspection, regulation, and analysis. The information is often produced at the tail end of a process and used for making manufacturing improvements. However, by integrating metrology techniques into manufacturing processes, measurement data can be utilized in a closed loop system to provide useful information.

Large scale, portable metrology techniques offer solutions to measurements that would otherwise be difficult to obtain. The introduction of coordinate measuring systems (CMSs) and portable, accurate measurement devices allows for more informative measurements on large components to be acquired. A specific challenge is that the shapes of large objects are influenced by the way that they are supported. As explored in this thesis, experimentation and finite element analysis can be used to predict and quantify the extent of distortion that is reflected in a component's measured state.

Industries such as energy, shipbuilding, and aerospace can benefit greatly from the measurement capabilities offered through coordinate metrology techniques. Employing these devices and new methodologies to large scale manufacturing can be a critical factor in the competitive industries when meeting demanding tolerances and performance requirements.

The motivation for the thesis was to demonstrate the methodology of integrating advanced metrology techniques and digital data structures into an existing manufacturing process to reduce time, cost, and effort. Specifically, the methodology was demonstrated in the assembly and alignment of a power plant generator Frame and Stator Core.

Generators consist of three main components, being the Rotor, Stator Core, and Frame. A generator is assembled by first aligning and mounting the Stator Core inside the Frame. Then, the Rotor is mounted inside the Stator Core. The thesis focused on the measurement and assembly of the Stator Core and Frame.

Both the Frame and Stator Core were measured individually using a laser tracker. After processing the individual component measurements, they were combined into a digital framework. The Frame and Stator Core were digitally aligned and used to calculate the dimensions of alignment shims that would be pre-manufactured for their physical assembly. The methodology validated the feasibility of using digital assembly for pre-manufacturing shims and showed how the exiting process could be improved.

CHAPTER 2. LITERATURE REVIEW

Advances in large scale metrology (LSM) have been driven by increasing part dimensions and demanding performance requirements in several manufacturing industries. Manufacturers have begun utilizing new LSM techniques as developments in metrology instrumentation have made large scale measurement tasks more feasible, [1] . In particular, the energy industry can benefit greatly from the application of new LSM concepts and technologies, [2] . However, all large scale manufacturers face specific challenges. Schmitt [3] discusses these challenges as they relate to increasingly demanding industrial requirements. Gravitational sag, small batch productions, and changing measurement environments are all identified as challenges inherent with the measurement tasks.

As companies move away from traditional manufacturing inefficiencies, such as inflexible jigs and part rework, attention has been directed towards measurement assisted assembly (MAA), [4] . In MAA, "components are measured pre-assembly and the measurement data is used to…the manufacture of predictive shim[s]." MAA is generally related to part-to-part assembly strategies that include predictive shimming, fettling, and drilling. Predictive shimming is identified as predictively making shims for filling gaps between two assembled components. Maropoulos [5] described part-to-part assembly as a process of performing all fabrication operations pre-assembly to allow for a one-way assembly.

Cai [6] addresses the importance of having measurability in mind during a product's early design by considering its part dimensions, environmental conditions,

measurement locations, and instrument capabilities. Cai [7] also writes that metrology is traditionally perceived as a verification that follows production, being separated from manufacturing. As manufacturing encounters new challenges, integrating metrology with manufacturing systems will become necessary, [4] [8] .

An example of metrology integrated with manufacturing was performed by Witte [9] in the assembly of airplane structure elements, where a 3D scanner was used in conjunction with a robotic system to measure and constrain flexible, fuselage panels during their assembly. In application, parts may need to be forced into their functional state as the metrology of non-rigid components in manufacturing can be complex, [10] .

In a project called the Light Controlled Factory, Maropoulos [11] identified several key instruments used for enabling MAA, including laser trackers, photogrammetry, and indoor GPS. These instruments, each suited for specific measurement tasks, employ optical techniques that enable the measurement of objects too large for conventional CMMs, [12] . However, Sawyer [13] describes the operating principles and technology of laser trackers and recognizes the instruments as the “tool of choice” for measuring large components.

In addition to improving product quality, integrated metrology can have valuable economic benefits, [14] . Carmignato [15] analyzed some industrial cases to quantify the economic impact of metrology, especially in small batch productions. Particularly, “metrology may allow substantial economic benefits in manufacturing when used simultaneously during production…enabling closed-loop control of the manufacturing process.”

Research was conducted by Fuzhou [18] regarding the uncertainty of MAA for aircraft wing-fuselage alignments, where the two main error sources were setup variation and instrument uncertainty. Research has also been done on the estimation of measurement uncertainty for portable LSM systems that use a reference network to tie multiple instruments together into a common coordinate system, [19] [20] [21] .

CHAPTER 3. CURRENT ALIGNMENT PROCESS

3.1. Current Frame to Stator Core assembly

Generator assembly begins with aligning and mounting a Stator Core inside its Frame. The Stator Core, referred to as the "Core," is mounted inside the Frame via brackets. These brackets are welded to the sides of the Core and positioned such that their profiles enclose two rectangular bars, referred to as "springbars", on the inside of the Frame, as illustrated in FIGURE 3-1. The Core is approximately 1.5 m in diameter with a length of 6 m. The Frame is approximately 3.8 m in diameter with a length of 10.8 m.

The Cbeam is the generator assembly station and consists of a large cantilever support extending from a sturdy base. For assembly, the Core is placed on the cantilever beam which suspends it several meters above the shop floor. The Core is oriented such that its brackets are horizontal and its electrical leads are vertical. The Frame is slid over the Cbeam onto four hydraulic jacks, making no contact with the Core. The hydraulic jacks are stationed around the Cbeam and underneath the Frame supports, such that the Frame ribs do not touch the shop floor. The Frame is positioned such that its springbars slide through the brackets. The assembly process is illustrated on the left side of FIGURE 3-1.

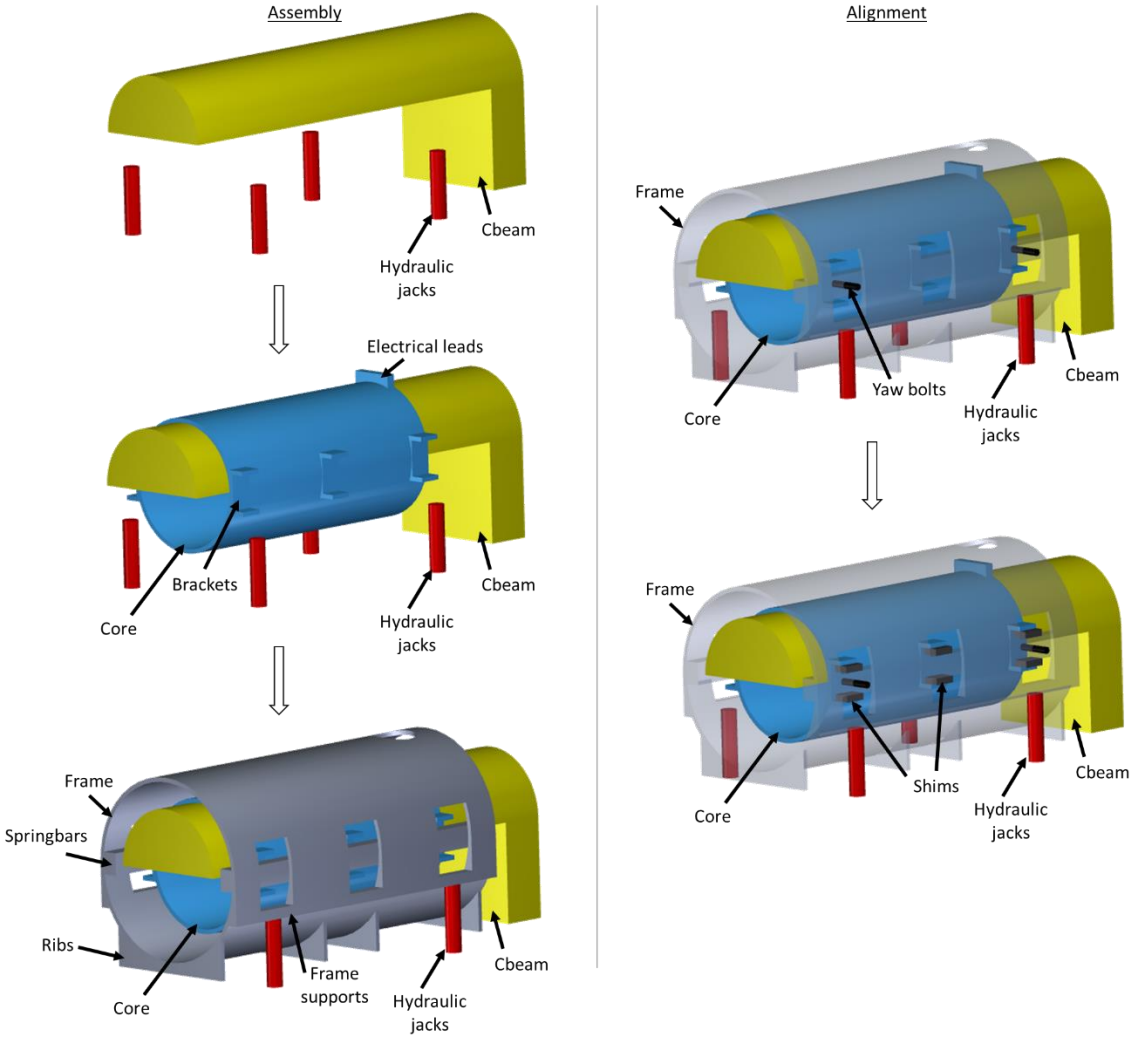

FIGURE 3-1: Cbeam assembly (left) and alignment (right) of a Frame and Core

For alignment, the Core remains stationary on the Cbeam while the Frame's position is adjusted. Axial adjustments are made by sliding the Frame with chain hoists attached to the Cbeam base. Vertical (Z), pitch, and roll adjustments of the Frame are made using the hydraulic jacks. Horizontal (Y) and yaw adjustments are made using yaw bolts that thread through the springbars and press against the brackets to slide the Frame. The yaw bolts are illustrated on the right side of FIGURE 3-1. The generator alignment nomenclature is presented in FIGURE 3-2, with a coordinate system (CS) drawn on the Frame.

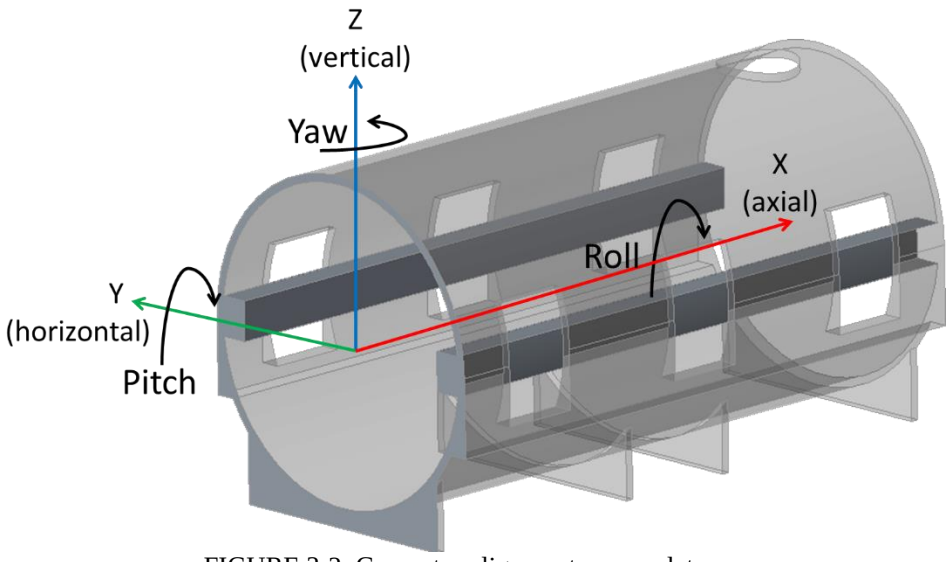

FIGURE 3-2: Generator alignment nomenclature

The assembly drawings do not call for the two component centerlines to be concentric, but rather prescribe vertical and horizontal displacements at their ends. Therefore, the current process uses an assemble-measure-move strategy to iteratively adjust the Frame so that its ends meet specified positions relative to the Core's centerline. Axial alignment from the ends of the components is also met per the drawings. A local CS is established on both components for measurement, while the final alignment is based on the Core CS.

Throughout the alignment procedure, the brackets do not touch the springbars, but rather are separated by gaps, both vertically and horizontally. After achieving an acceptable alignment between the Frame and Core, the vertical gap dimensions are measured using adjustable parallels and calipers. Shims are manufactured to these dimensions and inserted into the gaps, as illustrated in FIGURE 3-1. Finally, the shims are welded into the assembly, thereby locking the alignment in place. FIGURE 3-3 illustrates the relationship between the brackets, springbars, and shims.

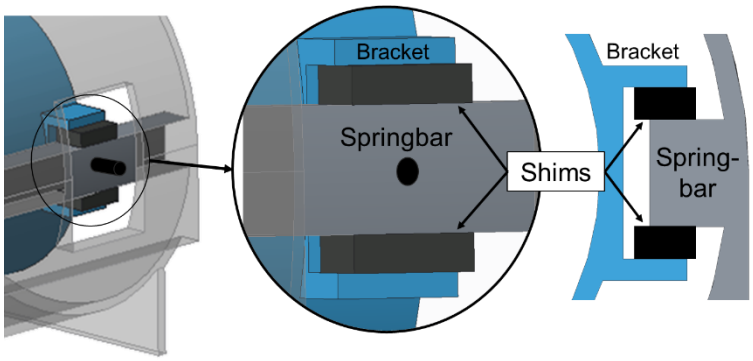

FIGURE 3-3: Shim placement between brackets and springbars

3.2. Current alignment method

The assembly and alignment procedures are performed in collaboration between the manufacturer and an external contractor. To measure the relative position of the Frame and Core, the contractor first performs measurements on the components prior to their assembly. Based on the measurements of specific features, the contractor establishes a local CS on each component. Points called “control points” are also measured on each component.

After the Frame and Core are placed on the Cbeam, the contractor re-measures the control points. In Spatial Analyzer software the contractor uses these control point measurements to locate the current positions of the Frame and Core through rigid body transformations. In the digital assembly, the contractor determines the relative position of the Frame centerline relative to the Core centerline. The positional coordinates of the Frame centerline endpoints are reported as relative to the Core’s local CS.

Based on these values, the contractor prescribes physical adjustments of the Frame’s position which are then made by the manufacturer. Measuring the control points

on the components, evaluating their alignment, and prescribing positional adjustments of the Frame is an iterative process, often taking several hours.

Upon achieving a successful alignment in tolerance, the contractor stops measuring and prescribing Frame adjustments. The manufacturer then measures the gaps between the brackets and springbars. The Core and Frame remain on the Cbeam while the manufacturer machines all the shims, which generally requires half a shift. Finally, the shims are slid into their places in the assembly and welded. The assembly is then removed from the Cbeam and placed elsewhere for further fabrication.

3.3. Opportunities for improvement

Three major opportunities for improvement in the current assembly process are identified.

1. An outside contractor is required to perform the measurements and alignment, requiring time and money. The contractor's travel causes delays in the generator manufacturing line and the whole process itself often takes several days to complete. By bringing the measurement skill in-house, the manufacturer has more control over the process. With an understanding of the current process and a knowledge of fundamental metrology principles, the manufacturer may eliminate the need for an external contractor.

2. The Cbeam jacks govern the repositioning of the Frame for alignment. The jacks are adjusted vertically by threaded collars on the jack bodies. Practical resolution in displacement is about 1/16 a turn by an operator, or 0.375 mm vertically. Therefore, controlled adjustments in the Frame's position less than 0.375 mm are not realistic. By

implementing the project's proposed process, the accuracy of the alignment would be primarily governed by measurement accuracy.

3. The Cbeam station is the only location where the generator assemblies are performed, putting it in the critical path of manufacturing. By pre-manufacturing the shims to fill the gaps, time spent on the Cbeam station could be greatly reduced.

CHAPTER 4. DIGITAL ASSEMBLY METHOD

This project developed a proposed process for pre-manufacturing the shims for alignment. In addition to the contractor's measurements used to define the component centerlines, additional features necessary for shim calculation were also measured. These features were the Frame springbars and Core brackets. In the digital assembly process, the relationships between the springbars and brackets were extracted and used to prescribe shim dimensions. FIGURE 4-1 identifies the major contributors in enabling the digital assembly process. The project focused on measurement, analysis, mechanical assembly, and verification.

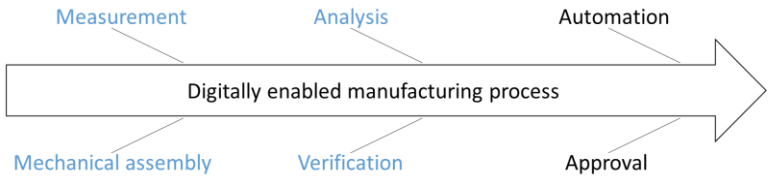

FIGURE 4-1: Project contributors

4.1. Measurement setup

Laser trackers and spherically mounted retroreflectors (SMRs) were used by the contractor in the current process, and the same devices were chosen for the proposed process. Other instruments such as a structured light scanner and a laser radar were considered, but not pursued. Spatial Analyzer (SA) metrology software was used for measurement and analysis.

Multiple laser tracker positions were required to measure all of the necessary features on the Frame and Core. Reference networks were established around the components to tie the multiple laser tracker positions together. A reference network is a series of common stable reference points that enable measurements from two or more

instrument positions to be combined into a common reference coordinate system through a best-fit transformation.

In the Frame reference network, drift nests were adhered to the inside surfaces of the springbars. For the Core, drift nests were adhered to the shop floor. Drift nests were puck-shaped kinematic mounts that held SMRs in place for repeatable measurements.

To mount the drift nests, the surface was first wiped with a clean rag. A wide piece of adhesive tape was applied to the clean surface. The drift nest was placed on top of the tape and hot glue was laid around its bottom edge. The drift nests had magnets to seat the SMRs. If a drift nest was moved during a measurement process, its reference point was rendered unusable. Therefore, care was taken to properly mount the drift nests. A mounted drift nest with and without an SMR is shown in FIGURE 4-2.

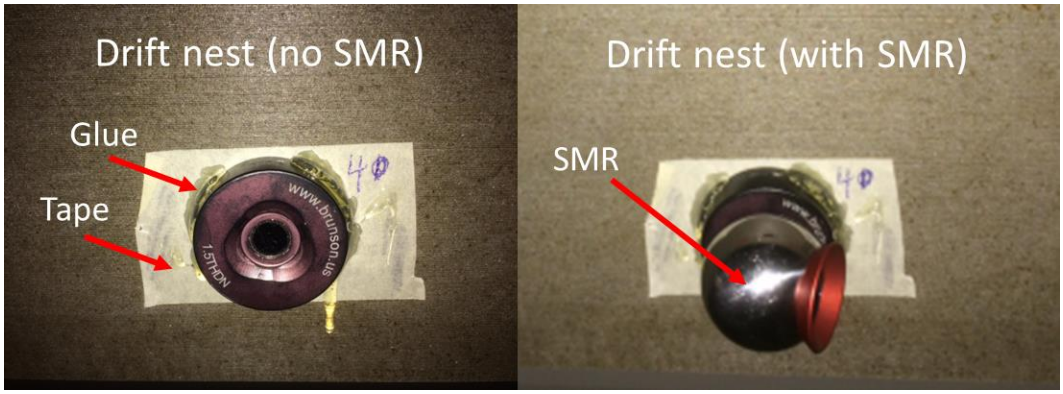

FIGURE 4-2: Drift nest attached to surface, without (left) and with (right) an SMR

4.2. Component nomenclature

The Core nomenclature is illustrated in FIGURE 4-3 as related to the Cbeam. The shop floor cardinal designated North and South, while the lead end (LE) defined the end of the Core that the electrical leads exited the windings. No leads exited from the

non-lead end (NLE). The Core brackets were numbered Bracket 1 through Bracket 6 and abbreviated as B1 through B6, respectively.

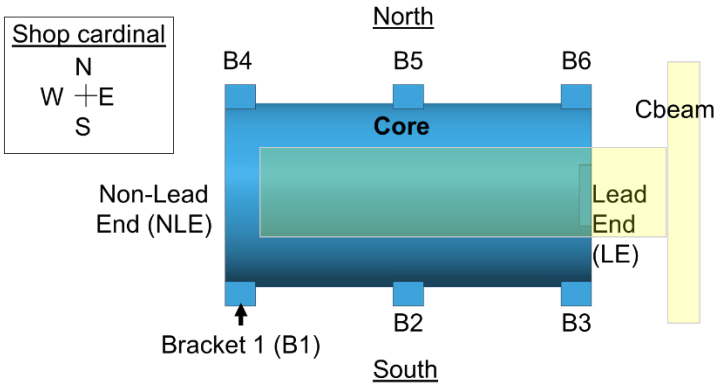

FIGURE 4-3: Core nomenclature as related to Cbeam

The Frame nomenclature is illustrated in FIGURE 4-4 as relative to the Core. The shop floor cardinal designated the North and South springbars and a hole through the top of the Frame for the electrical leads designated the LE. The Frame ribs were at the bottom of the component, while its supports were along its sides. The Core bracket locations are labeled on the springbars respectively.

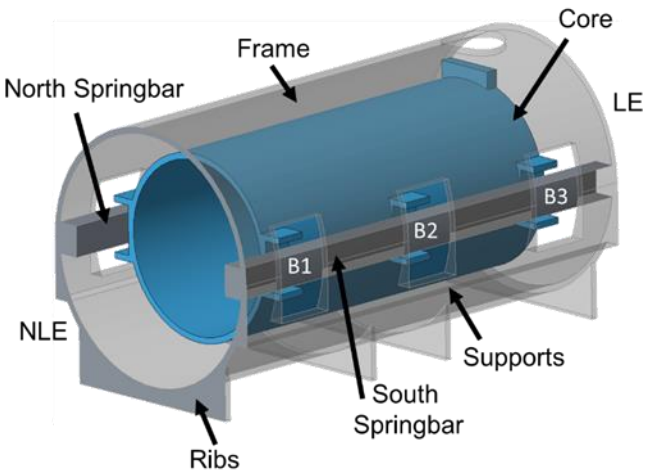

FIGURE 4-4: Frame nomenclature as related to the Core

4.3. Frame measurement strategy

All of the features measured on the Frame are illustrated in FIGURE 4-5. TABLE 4-1 lists all the Frame features that were measured, their purpose, how many points were usually recorded, and what geometry was calculated. The number of data points was kept to a minimum to reduce measurement time and analysis. During the project, Model 1 and Model 2 generators were measured and had minor differences in their measurement strategy. The typical Frame measurement floor plan for the proposed process is shown in FIGURE 4-6.

The following sections describe how the features on the Frame were measured and how the data was processed for digital assembly.

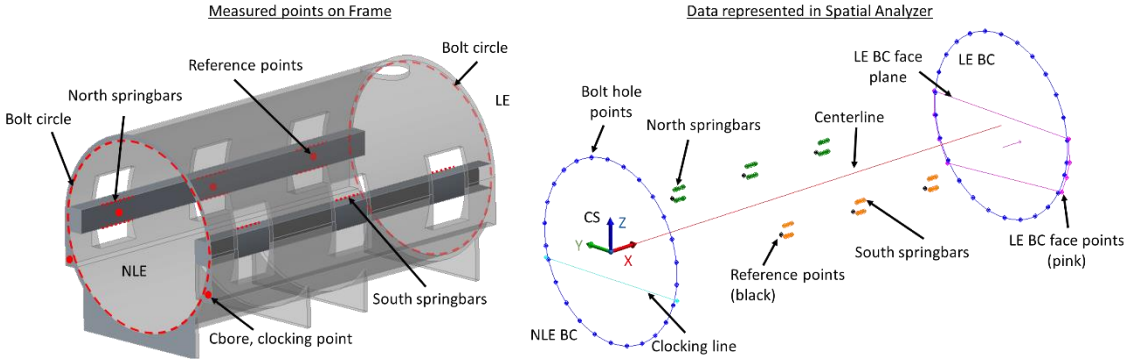

FIGURE 4-5: Measured features on a Frame

TABLE 4-1: Measured features on a Frame

Feature	Purpose	Description of data points	Fitted geometry
NLE bolt circle enter	CS origin	25 bolt holes (every 5th)	Circle
NLE clocking points	CS +Y direction	2 points in Cbores	Line
LE bolt circle center	CS +X direction	25 bolt holes (every 5th)	Circle
LE BC face	Core axial positioning	~8 points on end face	Plane
North springbar	Shim dimensions	5 points top and bottom at each bracket	Lines
South springbar	Shim dimensions	5 points top and bottom at each bracket	Lines
Reference points	Instrument transformation	6 reference points (1 at each bracket)	N/A

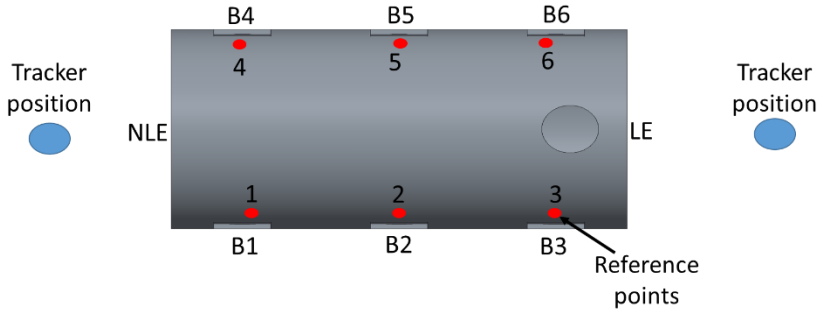

FIGURE 4-6: Frame measurement setup floor plan

The Frame CS was established such that the origin was the NLE bolt circle (BC) center, the +X axis passed through the LE BC center, the +Y axis was parallel to a line established between two clocking points on the NLE, and the +Z axis was the vector product of the X and Y axes.

4.3.1. Frame bolt circles

The Frame had circular bolt hole patterns on its ends that were referred to as the NLE and LE bolt circles (BCs). The BCs were measured by seating a 1.5" SMR into the bolt holes as shown in FIGURE 4-7. Each BC consisted of 128 bolt holes, but only 25 were measured. A circle was fit to the measured bolt holes and no probe offsets were

applied. The Frame CS origin was located at the NLE BC center. The Frame's centerline was defined by the NLE and LE BC centers.

FIGURE 4-7: SMR in Frame bolt hole

As the project progressed, the number of bolt holes per BC varied. Eventually, the chosen number of measured bolt holes was based on contractor knowledge and confirmed through basic analysis. The analysis evaluated how the center coordinate of the BC deviated as the number of measured bolt holes changed. From the measurements of all 128 bolt holes on a single BC, individual circles were fit, using a least squares approach, to groups of every 3rd, 5th, 7th, and 9th data point, as shown in FIGURE 4-8. Coordinate deviations were calculated for each circle center to the center of the BC fitted to all the bolt holes.

The maximum deviation was 0.07 mm for every 5th bolt hole, as shown in TABLE 4-2. The results are based only on one set of data and therefore are not a statistically sufficient sample. However, they do give an idea of how minimally the BC center changes depending on the number of bolt holes measured. Based on the findings, experience, and the need to limit measurement time, it was decided that every 5th bolt hole would be measured. The Matlab code for the analysis is provided in APPENDIX A.

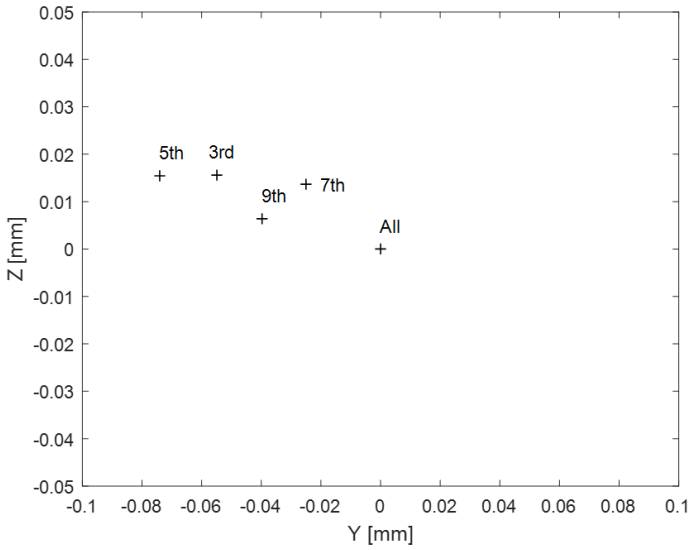

FIGURE 4-8: BC centers fit to a varying number of measured bolt holes

TABLE 4-2: BC center coordinates and deviations

Bolt holes (128 total)	Y coordinate	Z coordinate	Deviation magnitude from All
All	0.00	0.00	0.00
Every 3rd	-0.05	0.02	0.05
Every 5th	-0.07	0.02	0.07
Every 7th	-0.03	0.01	0.02
Every 9th	-0.04	0.01	0.04

4.3.2. Clocking line

In addition to the BCs, 2 points, referred to as clocking points, on the NLE were measured to help define the Frame CS. For the Model 1 Frame, the clocking points were measured by seating the SMR into holes, referred to as Cbores. For Model 2, the clocking points were small holes on the NLE. A line was created between the two points and used to define the Frame CS clocking point, as shown in FIGURE 4-5.

4.3.3. LE BC face

Several data points were recorded on the LE BC face using a bare SMR on the surface as shown in FIGURE 4-9. A plane was best-fit to the data through the probe center and no probe offset was applied. Probing offsets were unnecessary if not applied to either component's LE face measurements because the centroid of the plane was used for aligning the Frame to the Core in digital assembly. The LE BC face data points are labeled in FIGURE 4-5.

FIGURE 4-9: SMR on BC face

4.3.4. Springbars

As mentioned above in Section 3.1, the springbars were rectangular beams extending nearly the entire length of the Frame. To locate the springbars relative to the Frame CS, data points were measured along the top and bottom edges where the Core brackets were mounted. Five data points were equally spaced along the edges as illustrated in FIGURE 4-5 and listed in TABLE 4-1. The SMR was paired with an edge nest and seated onto the springbar edges as illustrated in FIGURE 4-10.

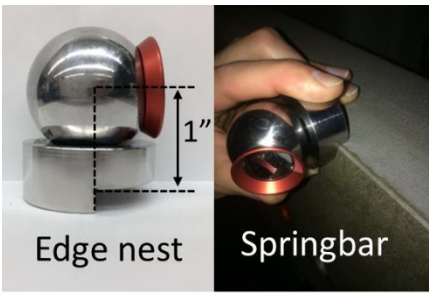

FIGURE 4-10: SMR with edge nest on springbar

A line was fit to each set of springbar points and a probing offset was applied. The lines were shifted ±25.4 mm along the Y axis of the Frame CS to account for the edge nest’s planar offset, as illustrated in FIGURE 4-11. The offset was applied respectively to the North and South springbars along the +Y and –Y directions. The offset lines were used for shim calculation.

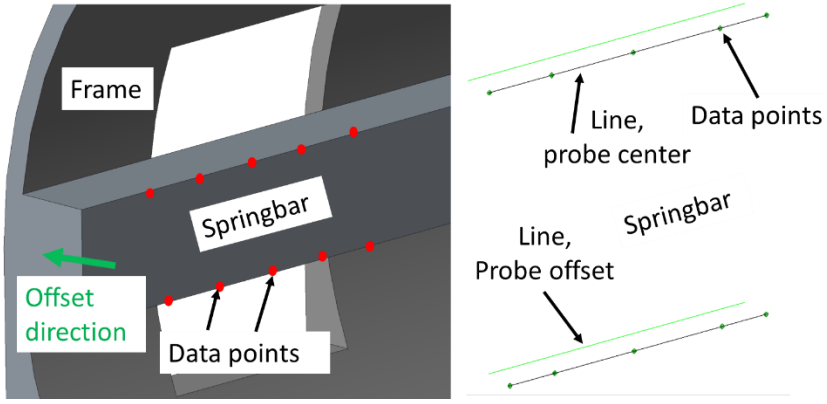

FIGURE 4-11: North springbar measurements at B4 location, illustrated (left) and represented in SA (right)

4.3.5. Reference network

To tie the NLE and LE tracker position data sets together, a reference network was establish on the Frame. In total, six drift nests were mounted to the inside surfaces of the springbars using the method describe in Section 4.1. The drift nests were placed

on the springbars at the bracket locations as illustrated by red dots in FIGURE 4-6. All six reference points were visible from both tracker positions.

4.4. Core measurement strategy

The measured features on the Core are illustrated in FIGURE 4-12. TABLE 4-3 lists all the Core features that were measured, their purpose, how many points were usually recorded, and what geometry was calculated. The measurement floor plan is shown in FIGURE 4-13. The Core was always measured while supported on two v-blocks on the shop floor. In general, the number of recorded data points was kept minimal to reduce measurement time.

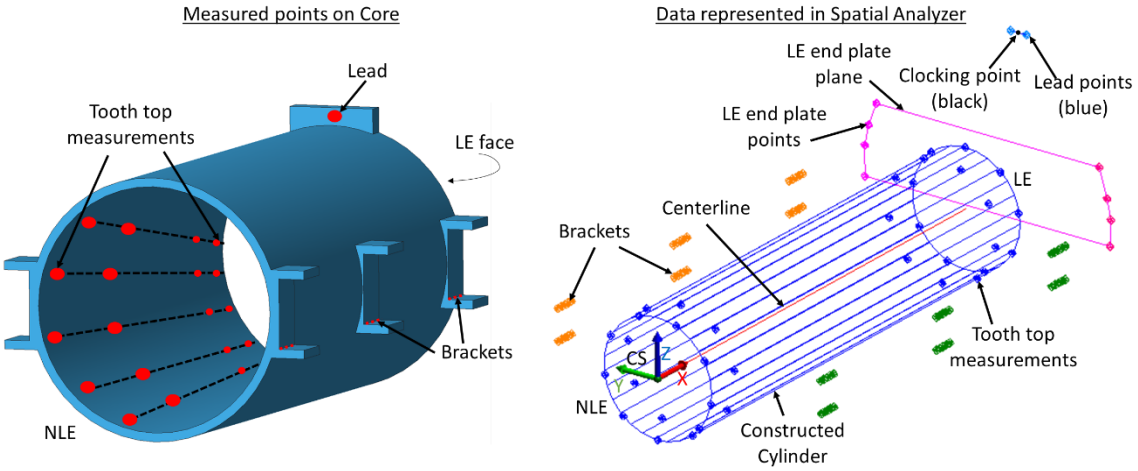

FIGURE 4-12: Measured features on the Core

TABLE 4-3: Measured features on the Core

Feature	Purpose	Description of data points	Fitted geometry
Tooth tops	CS origin & +X direction	~36 tooth top locations	Cylinder
Lead	CS +Z direction	2 points in leads	Line
LE face	Core axial positioning	8-12 points on end plate	Plane
North brackets	Shim dimensions	5 points, top and bottom at each	Lines
South brackets	Shim dimensions	5 points, top and bottom at each	Lines
Reference points	Instrument transformation	6 reference points (glued on shop floor)	N/A

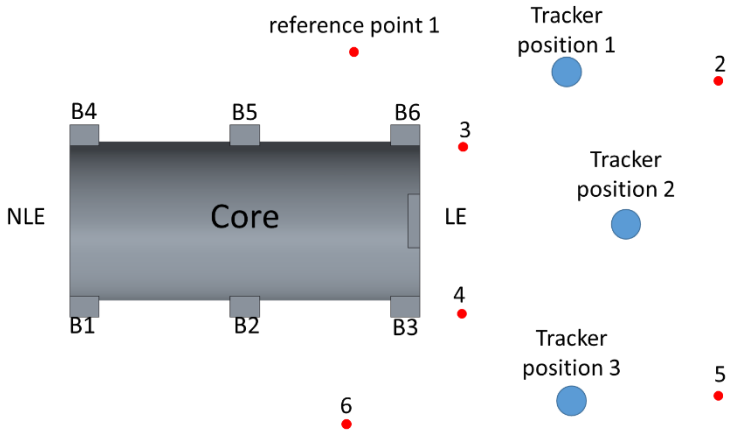

FIGURE 4-13: Core measurement setup floor plan

The Core CS was established such that the origin was located at the NLE endpoint of the tooth top cylinder, +X axis was coincident with the cylinder axis, +Z axis was clocked to the center of the Core lead, and +Y axis was defined by the right hand rule.

4.4.1. Core cylinder

The same method used by the contractor to define the Core's centerline by its inner cylinder was applied in the proposed process. In total, 4 circles of at least 7 points each were measured at different axial positions along the Core. Two circles were located towards the NLE and two towards the LE. All cylinder measurements were recorded from the second tracker position. FIGURE 4-14 shows how the SMR was placed on "tooth tops" for measurement.

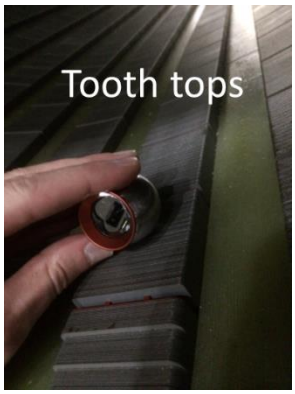

FIGURE 4-14: SMR on tooth tops

In SA a cylinder was fit to all of the tooth top measurements and no probing offsets were applied. The center axis of the cylinder was used to define the Core's centerline. The cylinder's NLE endpoint represented the origin of the Core CS.

4.4.2. Core CS Clocking point

The clocking point of the Core CS, was measured from the second tracker position. On each Core, a metal lead with a series of holes extended from the LE. Two points were measured on the lead by seating a bare SMR into the holes. The midpoint of a line connecting these points represented the clocking point of the Core CS. The measurement is illustrated in FIGURE 4-15.

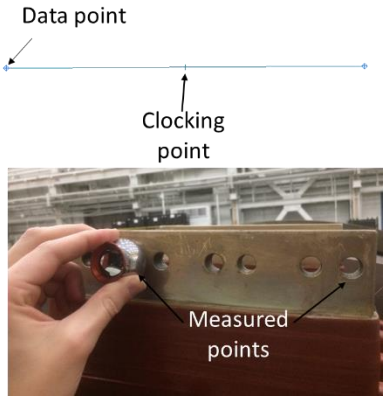

FIGURE 4-15: Clocking point measurements

4.4.3. Core LE face

Several points were measured on the Core's LE face. The LE faces were thick, steel rings bolted at the ends of the Core. Typically 8 points total were measured on the LE face using a bare SMR from the first and third tracker positions. FIGURE 4-16 shows how the points were measured. After tying the data together, a plane was fit to the points and no probe offset was applied. The centroid of the plane was used for axial alignment to the Frame in digital assembly.

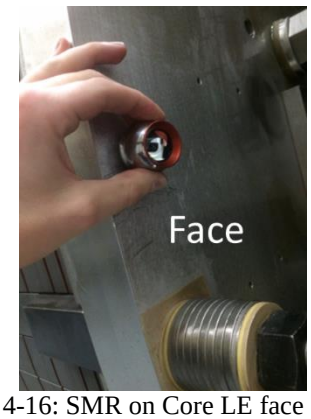

FIGURE 4-16: SMR on Core LE face (end plate)

4.4.4. Core bracket surfaces

To locate the bracket surfaces relative to the Core CS, points were measured along the top and bottom inside corners using a bare SMR, as shown in FIGURE 4-17. Five points were measured along each corner, with the first and last being near the bracket outer edges.

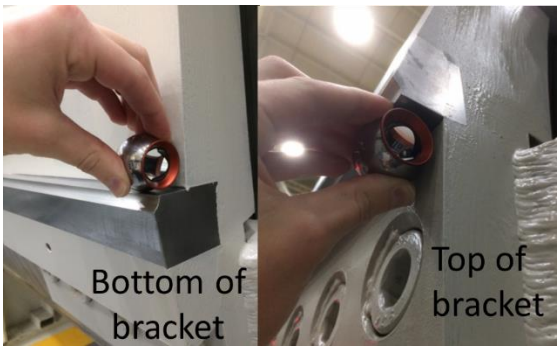

FIGURE 4-17: SMR on inside bracket corners;
bottom (left) and top (right)

Lines were fit to the top and bottom points for each bracket. Each line was offset ±25.4 mm along the Z axis of the Core CS so the data represented the top and bottom bracket surfaces. The offset is shown in FIGURE 4-18. The endpoints of the bracket lines were used for shim calculation.

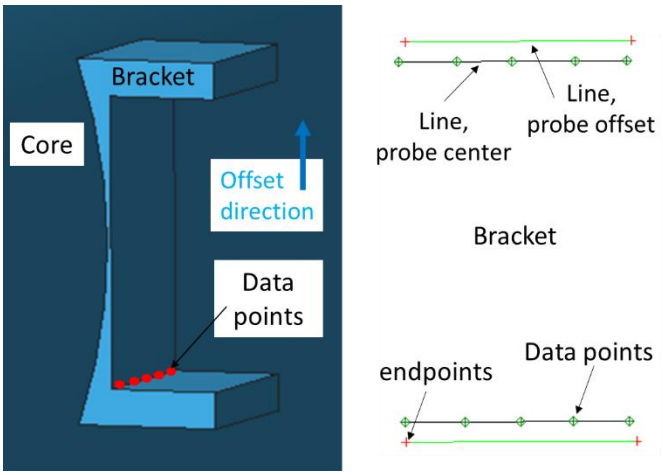

FIGURE 4-18: Bracket measurements illustrated (left) and represented in SA (right)

4.4.5. Reference network

Referring to FIGURE 4-13, six reference points were used to tie the data together. The drift nests were adhered to the shop floor. From the second tracker position all the reference points were visible. Due to line-of-sight, the first and third tracker positions were only able to measure reference points 1-5 and 2-6, respectively. All the tracker positions were tied together through the second tracker position.

4.5. Shim calculation

Shim calculation began by independently processing the Frame and Core measurement data into their feature geometries. A local CS was established on both components. A complete representation of the data processing is illustrated in FIGURE 4-19.

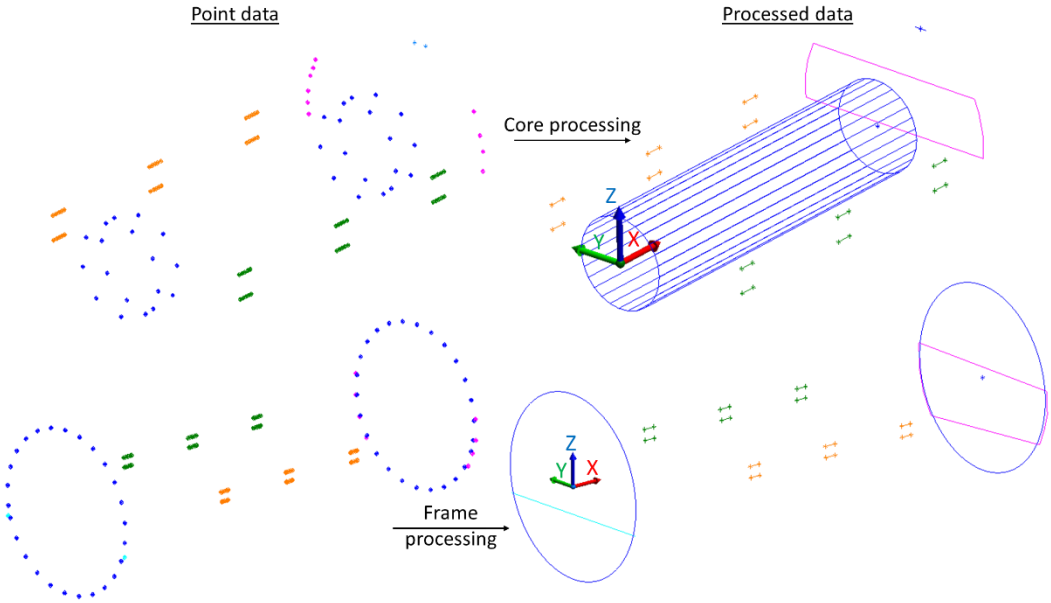

FIGURE 4-19: Core and Frame data processing

Next, the components were imported into a common file and their CSs were made coincident. The first step in the digital alignment was to satisfy the axial direction along the component centerlines. The Core data was shifted along the X axis to meet the specified dimension between the Frame LE BC face and the Core LE face. The Model 1 and Model 2 generator axial dimensions were 2267 mm and 2105 mm, respectively. FIGURE 4-20 shows this step in the alignment using a Model 1 for representation.

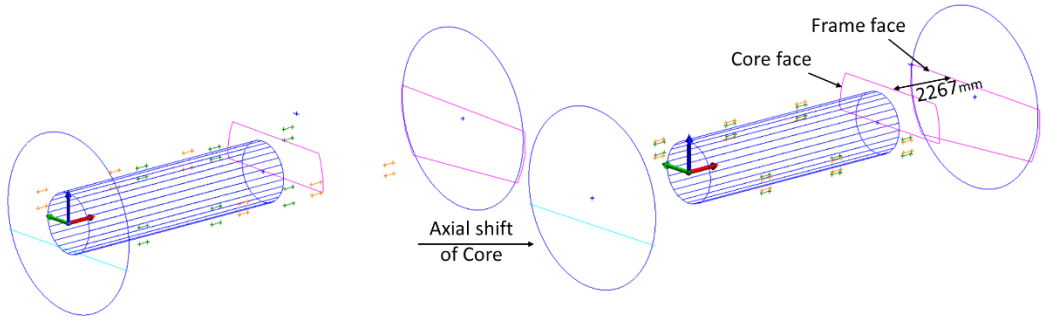

FIGURE 4-20: Axial alignment of Frame and Core

The next step for digital alignment was to vertically translate the Frame and pitch it about the Y axis of the Core CS. Nominal alignment of the components did not require

the centerlines to be coincident. Rather, vertical coordinates were prescribed to the Frame BC centers. If the digital alignment matched the nominal specifications, it was called a Case A alignment. Other digital alignments, Case B and Case C, are discussed later in the thesis. Case A alignment is illustrated in FIGURE 4-21**.**

In summary of the alignments, the Y, yaw, and roll were constrained by the initial CS overlay, the X was satisfied by the axial shift of the Core, and the Z and pitch were constrained by vertically shifting the Frame.

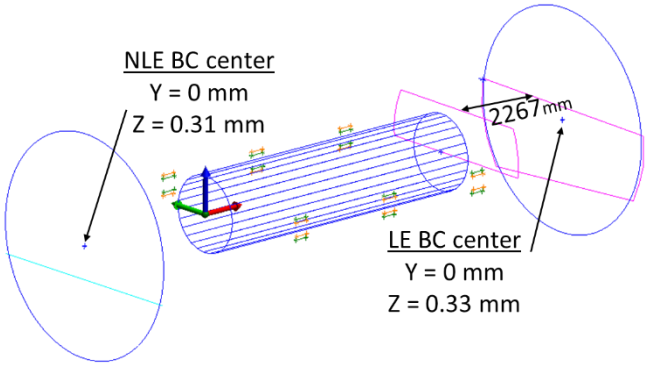

FIGURE 4-21: Final digital Case A alignment

After completing the digital assembly, the shim dimensions were calculable. The shim dimensions were defined by the distances between the bracket endpoints and their respective springbar lines. The distances were reported in X, Y, and Z deltas. The Z delta values were the shim dimensions. The relationship between the bracket endpoints and the springbar lines is illustrated in FIGURE 4-22.

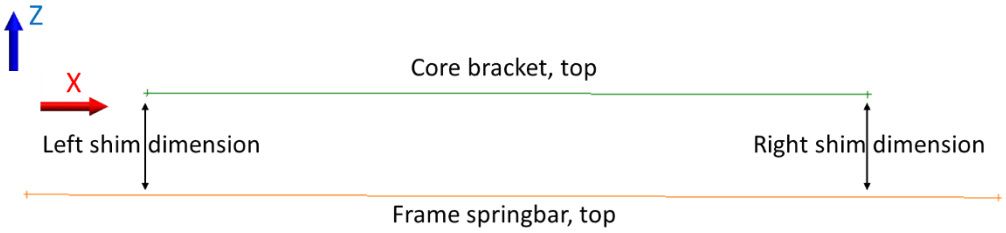

FIGURE 4-22: Bracket endpoints to springbar line relationships, viewing Top.

Four dimensions were calculated per bracket, totaling 24 dimensions for an entire generator. The locations of each shim dimension on a single bracket are illustrated in FIGURE 4-23. Left, right, top, and bottom were named as if viewing a bracket face on from outside the Frame. Therefore, each shim had a left and right dimension (i.e. Bracket 1 Top Left and Bracket 1 Top Right, or Bracket 1 Bottom Left and Bracket 1 Bottom right). Generally, a slight taper was found between the left and right dimensions.

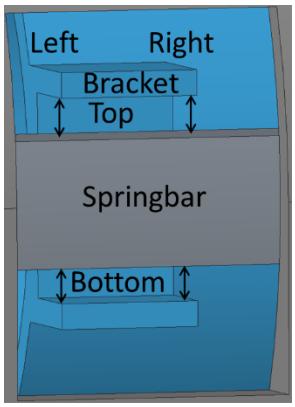

FIGURE 4-23: Shim dimensions at each bracket

CHAPTER 5. MODEL 1 DIGITAL ASSEMBLY RESULTS

The shim dimensions produced by the proposed process were referred to as "predicted" dimensions. The shim dimensions produced from the current process after the contractor aligned the components were referred to as "ordered" dimensions.

Ideally, the difference between predicted and ordered shim dimensions would have been zero. The closer they matched, the more likely that the predicted shims would have resulted in the same physical alignment as achieved by the current process. Through the project, a total of six generators were measured using the proposed process. For each, all 24 shims dimensions were compared to the current process.

5.1. Model 1 shim results

The shim results compared the difference between the predicted and ordered shim dimensions. As an example, let the Bracket 1 Top Left shim dimension be equal to 38 mm. After the contractor physically aligned the generator, the same dimension was ordered to be 36 mm. The difference between the values would be 2 mm (38 mm – 36 mm). Shim differences were always calculated such that the ordered value was subtracted from the predicted.

Before shim dimensions were calculated, all digital assemblies were aligned to replicate the alignment achieved by the contractor in the current process. This was referred to as a Case B digital alignment and used for comparing shims between the two processes. In physical assembly, the contractor did not achieve a perfectly nominal alignment, but simply attempted to make Y and Z offsets for both the NLE and LE BC centers within the specified tolerance band. The tolerance for both the Y and Z

coordinates of Model 1 generators was 0.508 mm. In digital assembly, axial alignment of the Frame and Core was always nominal.

The complete list of shim differences for the Model 1 generators are in APPENDIX B. The Model 1 shim results are summarized in TABLE 5-1. The generator number, Frame's support condition, and date measured are provided. The "Support" column lists how the Frame was supported when its measurements were taken for the proposed process. "Shim: Case B Predicted – Ordered" indicates the differences between predicted and ordered values, when the digital assembly was oriented for Case B alignment. The maximum and average absolute values of the shim differences are listed.

The final column titled "Gap: Case B Predicted – Ordered" evaluates the difference in the total gap on the left and right sides of the brackets. Total gap was determined by the sum of the Top Left and Bottom Left, or Top Right and Bottom Right, shim dimensions for a single bracket. For each bracket two total gaps were calculated, resulting in 12 values for each generator. Total gaps were calculated for both the predicted and ordered dimensions and their difference in value was reported with the shim differences. The maximum and average absolute values of the total gaps are listed.

TABLE 5-1: Shim results for all Model 1 generators

Generator	Support	Date	Shim: Case B Predicted - Ordered (mm)		Gap: Case B Predicted - Ordered (mm)	
			Max.	Avg. (abs)	Max.	Avg. (abs)
A1	Ribs on wood	March 9, 2017	0.45	0.20	0.24	0.07
A2	Ribs on wood	March 20, 2017	0.99	0.36	0.25	0.09
A3	Parrallels	May 2017	1.15	0.64	0.10	0.02
A4	Ribs on plastic	July 2017	1.21	0.54	0.22	0.07

In the Support column, “Ribs on wood” indicates that the Frame ribs were braced on top of wooden boards on the shop floor. “Ribs on plastic” indicates that the Frame ribs were placed on 50 mm thick plastic sheets on the shop floor. “Parallels” indicates that the Frame was supported under its side supports by large metal parallels that extended the length of the Frame.

Model 1 shim results revealed a mismatch between the predicted and ordered shim dimensions. Initially, the differences were expected to decrease as the proposed process was refined and more measurements were performed. Nevertheless, the maximum difference increased, reaching 1.21 mm for Generator A4. The average absolute values also increased, reaching 0.64 mm for Generator A3.

Despite the differences in top and bottom shim dimensions, the total gaps to be filled by the shims, i.e. the sum of the top and bottom shim dimensions, showed little variation. Small average total gap differences such as 0.02 mm and 0.09 mm indicated that measurements of the local component geometries, e.g. Frame springbars and Core

brackets, were the same for both processes. This meant that the tracker measurements were likely not the main source of error in the shim differences.

Therefore, the shim differences likely resulted from changes in the relative locations of the springbars and brackets between measurement of the components on the ground and assembly on the Cbeam. The hypothesis was that differences in the Frame support conditions from the ground to the Cbeam changed its physical shape. Since the digital assembly and shim predictions were based on the ground support condition, the changed shape when supported on the Cbeam would have caused the gap dimensions to change. Further analysis was done to evaluate any non-rigid behavior of the Frame.

5.2. Case C alignment

Case C alignment was developed to evaluate rigid body variations in the Frame. It was achieved by positioning the Frame and Core such that the predicted shim dimensions at three corners matched their ordered counterparts. In particular, the Frame data was transformed so that the predicted Top Left shim dimensions at B1, B3, and B4 matched the ordered dimensions at the same locations.

Case C alignments began with the component centerlines concentric. The Core was then shifted along the X axis of the Frame CS to meet the axial alignment, as illustrated in FIGURE 4-20**.** Next, the Frame was shifted along the Z axis to match the predicted B1 Top Left shim dimension with the ordered. Finally, the Frame was pitched about the Y axis to match the B3 Top Left shim dimension and rolled about the X axis to match the B4 Top Left shim dimension. FIGURE 5-1 illustrates the rigid body

transformations used for matching the three corner shim dimensions in the digital assembly. The components are not shown initially concentric for illustrative purposes.

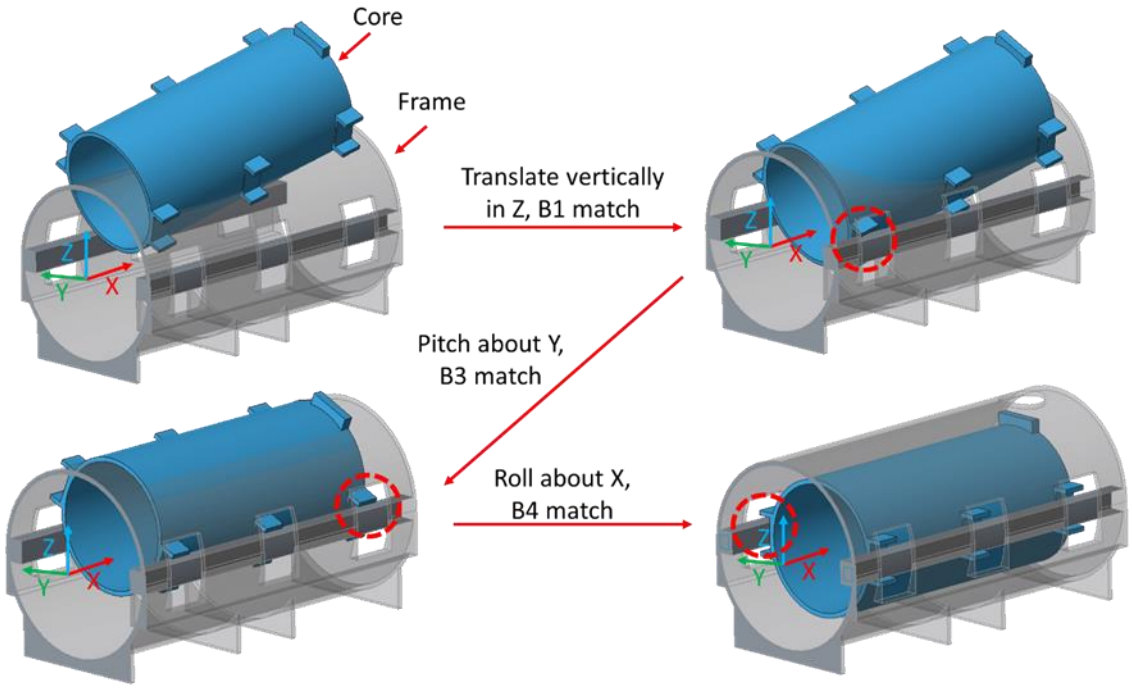

FIGURE 5-1: Case C rigid body transformations to match B1, B3, & B4 Top Left shim dimensions

After assembling the Frame and Core into the Case C alignment, any discrepancies between predicted and ordered shim dimensions would be a result of either incorrect digital alignment or changes in the shape of the generator components. By matching the three corner shim dimensions, the pattern of errors in the remaining shim dimensions provided insight to shape changes of the Frame. In particular, differences in the shim dimensions at B4, B5, and B6 indicated changes in springbar orientation relative to the brackets.

In other words, the Frame could have assumed different shapes between when the measurements were made on the shop floor and when the physical assembly took place

on the Cbeam. That is why TABLE 5-1 lists how the Frames were supported when they were measured for the proposed process.

5.3. Model 1 Case C results

In all Case C evaluations of Model 1 generators, the predicted and ordered shim dimensions at B4, B5, and B6 were found to vary. FIGURE 5-2 illustrates the Case C alignment results for Generator A4, where "Case C Predicted – Ordered (mm)" are the differences between the Case C predicted and the ordered shim dimensions.

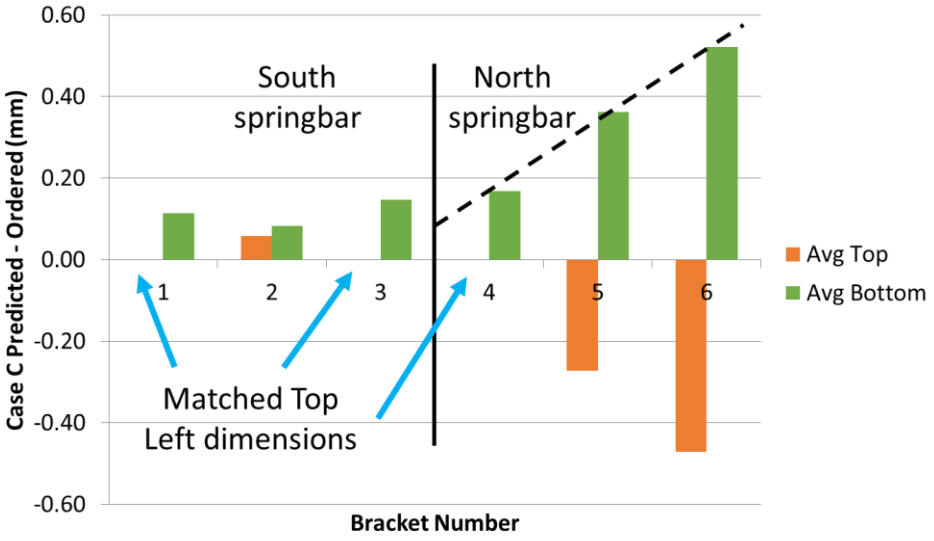

FIGURE 5-2: Generator A4 Case C shim results graph

The graph shows the average top and bottom shim differences for each bracket, where the blue arrows indicate the Top Left shim dimensions that were matched in performing the Case C digital alignment. A black line down the middle of the graph separates the brackets on the South and North springbars.

The sloping dashed line along the B4, B5, and B6 average bottom differences is what one would expect if the North and South springbars maintained their same basic shape, but changed their orientation or parallelism relative to each other. This meant that

the Frame changed shape when it was supported by the jacks at the Cbeam station, versus on the ribs and shop floor during measurement. These changes were causing the predicted and ordered shim dimensions to vary.

All four Model 1 Case C graphs are provided in FIGURE 5-3. Each reveals a similar sloping pattern from B4 to B6, indicating a change in the relative orientation of the springbars. While the data highlights shape changes in the Frame, it does not provide a sufficient means of quantifying the effects of its support condition. To further understand how the Frame was changing shape, another metric was developed based on the circularity of the NLE and LE BCs.

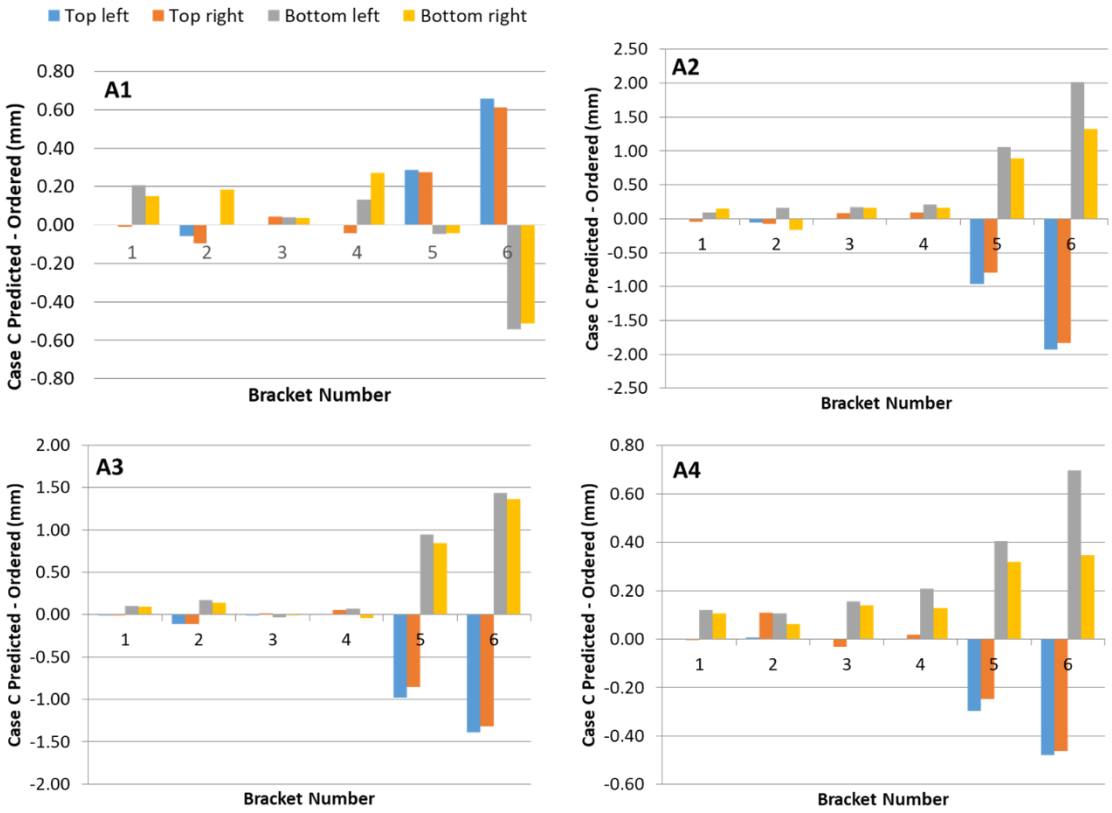

FIGURE 5-3: Model 1 generators Case C shim results graphs

5.4. Model 1 bolt circles

Frame BCs were evaluated by calculating the radial deviations of each single data point to a fitted circle. These were represented as colored vector groups, extending radially from the circle center. Outward vectors represented a positive deviation, while inward vectors represented a negative. The maximum outward deviation was used as a metric of circularity and roundness.

All of the Model 1 BCs revealed point deviations in elliptical patterns. Therefore, in addition to a circle, an ellipse was also fit. The angle of the ellipse's major axis relative to each Frame's CS was referred to as the BC's elliptic angle. The calculation is illustrated in FIGURE 5-4, where the Y axis represents the nominal angle of 0º. The

variable alpha, α, represents the elliptic angle of rotation. A clockwise rotation about the CS was a positive elliptic angle.

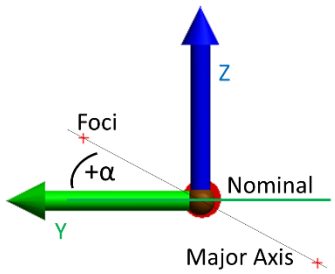

FIGURE 5-4: Elliptic angle calculation for BCs

It is important to note, that the elliptic angle of a BC does not mean that the end of the Frame was rotated by that amount. Rather, the angle of the major axis of the ellipse indicated that that the BC was distorted into an approximately elliptical shape, with a major axis at the reported angle. For analysis, the shape of the BCs were "untwisted" when the elliptic angle was approximately 0º. This definition of an untwisted Frame was only chosen for analysis and not used as the defining metric of twist.

The BC roundness and elliptic angles for all the Model 1 Frames measured with the proposed process are presented in FIGURE 5-5 and FIGURE 5-6. The generator number, Frame support condition, and who performed the measurements are listed below each BC. Each BC is reported along with its maximum roundness error and elliptic angle. A grey line illustrates the angle of the major axis. Vectors are shown with 1000x magnification. "Cbeam jacks" indicates that the Frame was supported on the Cbeam jacks after an Equal Pressure Lift, which is described is Section 6.1.

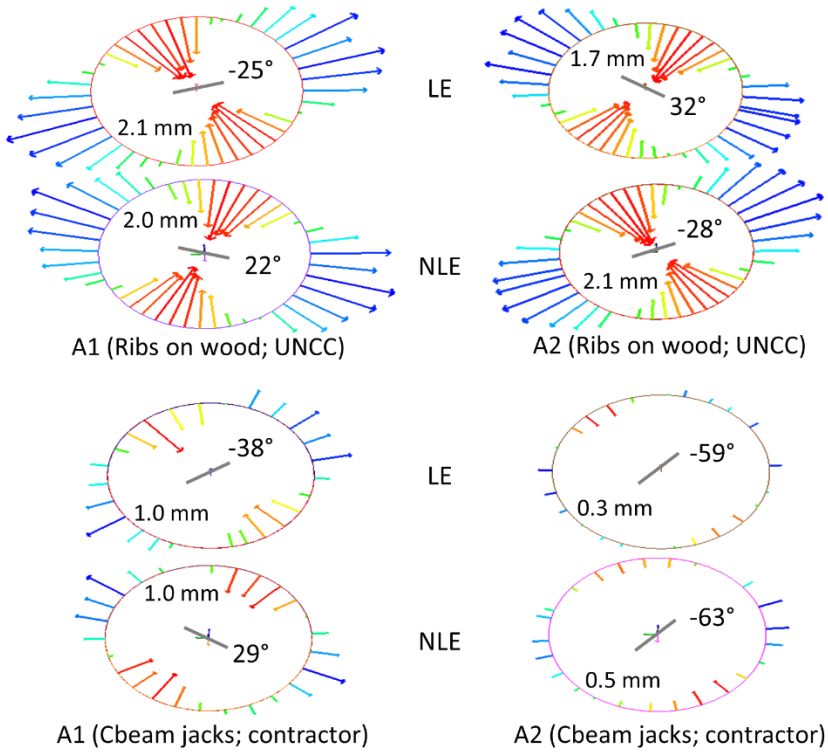

FIGURE 5-5: A1 and A2 BC roundness and elliptic angle, with contractor BCs

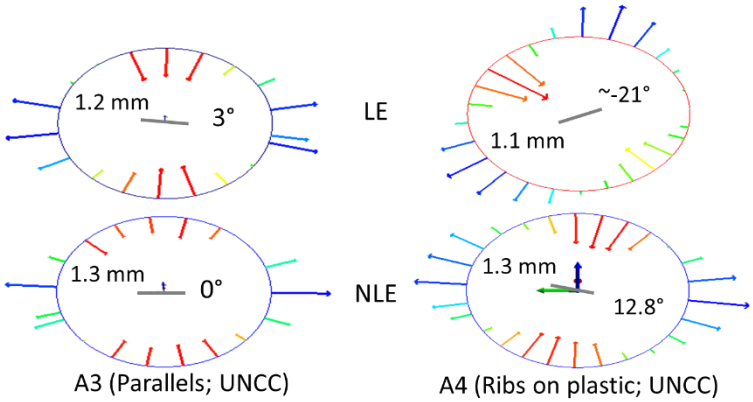

FIGURE 5-6: A3 and A4 BC roundness and elliptic angle

For Generator A1, the NLE and LE BCs show alternating elliptic angles. Both angles are similar, each being about ±25º. Also, both BCs have about a 2 mm roundness. The same correlations are found in Generator A2. The alternating elliptic angles in the BCs indicated that the Frames were experiencing torsional forces. Since these Frames

were supported on wood, they were subject to uneven surfaces that may have induced torsional forces. This would create the opportunity for one corner of the Frame to sit lower than the others and induce a twist.

Contractor measurements for Generators A1 and A2 revealed similar patterns in the BC distortions. Because roundness and elliptic angles were largely affected by measurement technique and the number of the bolt holes, it was difficult to draw a clear comparison between the proposed and current process BCs. However, both data sets indicated that the Frames experienced deformations when moved from the floor to the Cbeam jacks.

Generator A3, shown in FIGURE 5-6, had a roundness of about 1.2 mm for the NLE and LE. The elliptic angle, however, was nearly 0º for both BCs. The reason for the minimal elliptic angle was considered to be a result of the Frame being supported by parallels. This support condition may have mitigated any twisting. Nonetheless, the BC roundness was still affected by gravitational sag. Even though Generator A4 was supported on thick plastic pads below its ribs, it still experienced BC deformation. This resulted in roundness errors up to 1.3 mm and elliptic angles of -21º.

The conclusion drawn from this analysis was paired with the Case C alignment shim results to determine that the measured shape of the Frame is directly dependent on its support condition. A twisted Frame would alter the orientations of the springbars. This would directly affect the predicted and ordered shim dimensions if they were not based on the same shape of a single Frame. Therefore, it was important to understand

this relationship. The BC distortions led to further investigation of Frame rigidity through experimentation.

CHAPTER 6. MODEL 1 RIGID BODY EXPERIMENT

6.1. Objective and setup

The objective of the rigid body experiment was to evaluate non-rigid behavior of a Model 1 Frame. The A3 Frame was placed on the Cbeam jacks and put into its worst-case support conditions to demonstrate its non-rigidity. Three-point support conditions were created by raising and lowering the Cbeam jacks enough to relieve one jack from bearing any weight of the Frame. While the Frame was supported at only three corners, the unsupported corner sagged downward, inducing a twist through the component. In the experiment, four jack adjustments resulted in two support conditions, in addition to the nominal.

The nominal, "untwisted," support condition was chosen to be when all four jacks were equally loaded with the weight of the Frame. This was achieved through an Equal Pressure Lift by pressurizing all four jacks simultaneously. When the jacks were raised high enough, their locking collars were threaded down to set the height of the jacks. In this manner, because the jacks were on the same hydraulic circuit, they supported an equal amount of the Frame's weight.

Two sets of measurements were taken on the Frame in its nominal and worst-case support conditions. A laser tracker was positioned 10 m from the NLE of the Frame. On the NLE BC 19 bolt holes were measured. Additionally, 8 drift nests were mounted and measured along the inside surfaces of both springbars. The drift nests were placed arbitrarily along the length of the Frame springbars, as illustrated in FIGURE 6-1, using the method described in Section 4.1.

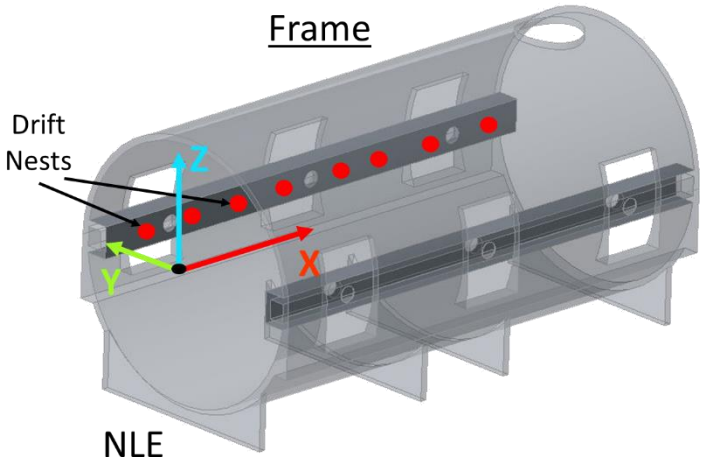

FIGURE 6-1: Drift nests distributed along the springbars

6.2. Results

6.2.1. Springbar planarity

Springbar planarity was used as a metric to analyze induced twist and the changing shape of the Frame in its different support conditions. Springbar planarity was calculated by first fitting lines through the points measured along each springbar. Then, a plane was fit to 3 of the 4 endpoints on these lines. The deviation of the fourth endpoint to the plane was the measure of planarity, as illustrated in FIGURE 6-2.

The line endpoints at the corners of the Frame were denoted based on the shop floor cardinal. A CS was established with its origin at the SW endpoint, the X axis passing through the SE endpoint, and the Y axis passing through the NW endpoint. Positive and negative deviations of the NE endpoint were above and below the plane, respectively. Nominal planarity was used as a reference, because the drift nests were arbitrarily placed on the springbars, and subtracted from the reported planarity values in TABLE 6-1.

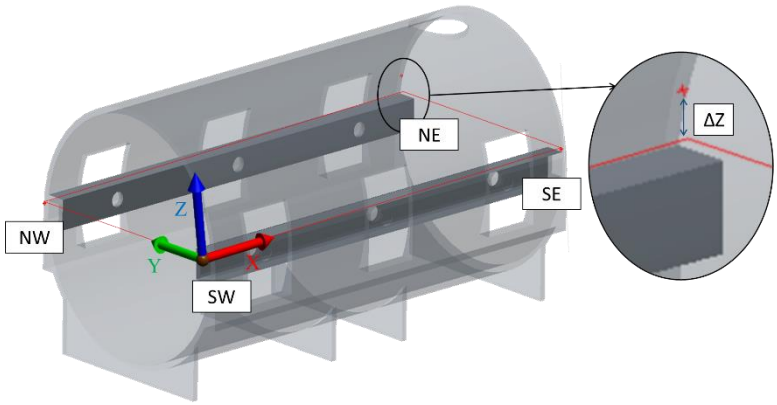

FIGURE 6-2: Springbar planarity evaluation

TABLE 6-1: Generator A3 springbar planarity deviations with nominal subtracted

Support condition	Jack adjustment	Planarity deviation of NE endpoint (mm)	Total displacement (mm)
NE jack relieved	NW up	-2.34	4.22
NE jack relieved	SW down	-2.35	
NW jack relieved	NW down	1.88	
NW jack relieved	SW up	1.87	

When the NE and NW jacks were relieved the planarity deviations were about -2.34 mm and 1.88 mm, respectively. This resulted in a total displacement of 4.22 mm. When the NE jack was relieved, the NE endpoint dropped below the springbar plane. Alternatively, when the NW jack was relieved, the NE endpoint was lifted above the plane. The alternating deviations show that the springbars were changing orientation in response to the changing support condition. Considering that a Model 1 generator alignment tolerance was ±0.508 mm, the displacement of the endpoints was significant.

6.2.2. Bolt circle analysis

The NLE BC roundness and elliptic angles in each support condition are presented in FIGURE 6-3. As described in Section 5.4, vectors are plotted on the circles

to illustrate point deviations. The CS for the experimental BC measurements was oriented with the Z axis clocked to a vertical bolt hole.

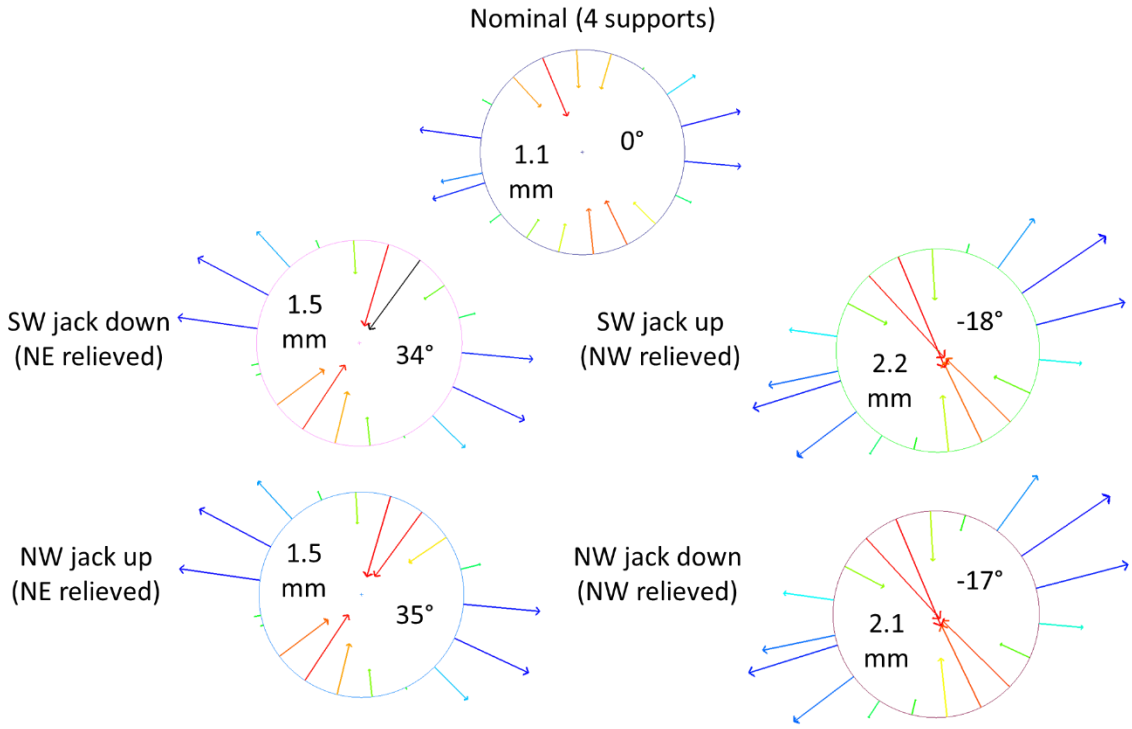

FIGURE 6-3: NLE BC roundness (1600x magnification) and elliptic angle for all support conditions.

The nominal BC produced an elliptic angle of 0º and a roundness of 1.1 mm. Even in an Equal Pressure Lift, the BC was still subject to deformation due to gravity. With the NE jack relieved, the NLE BC distorted to a roundness of 1.5 mm and elliptic angle of about 34º. When the NW jack was relieved, roundness was about 2.2 mm and the elliptic angle was about -18º. While the LE BC was never measured, based on previous BC measurements, it was assumed to have distorted similarly with alternating elliptic angle as the NLE.

6.2.3. Springbar straightness

A potential source of error in evaluating the springbar planarity was bending of the springbar. To understand how much their straightness changed between support conditions, the lines fit to the drift nest points were considered. The deviations of each point to its line was calculated and output as colored vectors. The deviation magnitudes are illustrated in FIGURE 6-4**.**

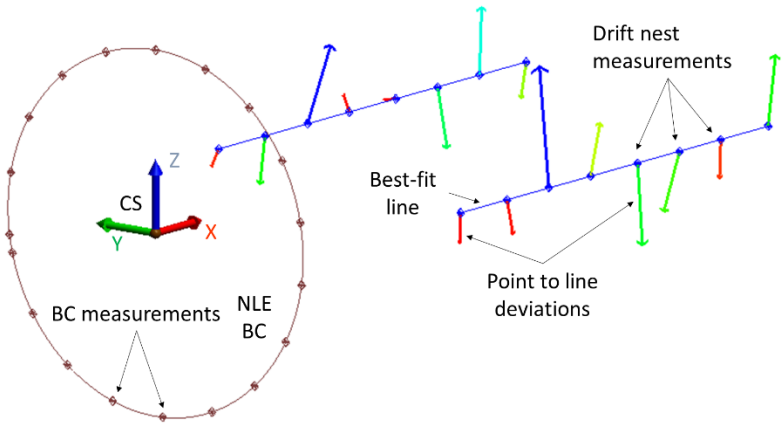

FIGURE 6-4: A3 drift nest line deviations, 200x vector magnification

The deviation vectors were reported in dx, dy, and dz delta components. Because the drift nests were placed arbitrarily in a straight line along the springbars, as noted in Section 6.1, the measurements of the nominal position served as a reference. The changes in point deviations were observed by subtracting the nominal.

$$Delta\ Z = dz_{[e.g.\ SW\ down]} - dz_{Nominal} \qquad \text{Equation 1}$$

and

$$Delta\ Y = dy_{[e.g.\ SW\ down]} - dy_{Nominal} \qquad \text{Equation 2}$$

Where,

$dz_{[e.g.\ SW\ down]}$ and $dy_{[e.g.\ SW\ down]}$ are the deviations of single points to the fit lines

after each jack adjustment, $dz_{Nominal}$ and $dy_{Nominal}$ are the deviations of single points to the nominal fitted line, and $Delta\ Z$ and $Delta\ Y$ are the differences between the individual deviations and nominal.

$Delta\ Z$ and $Delta\ Y$ are graphed in FIGURE 6-5 for all four jack adjustments. Dashed lines indicate the NE jack relieved support condition, while solid lines indicate the NW jack relieved support condition. In both the Z and Y axis directions, the springbars straightness changed by less than ±50 μm. This was the same range as the expected measurement accuracy of the laser tracker, so it was concluded that the springbars maintained their straightness through the experiment.

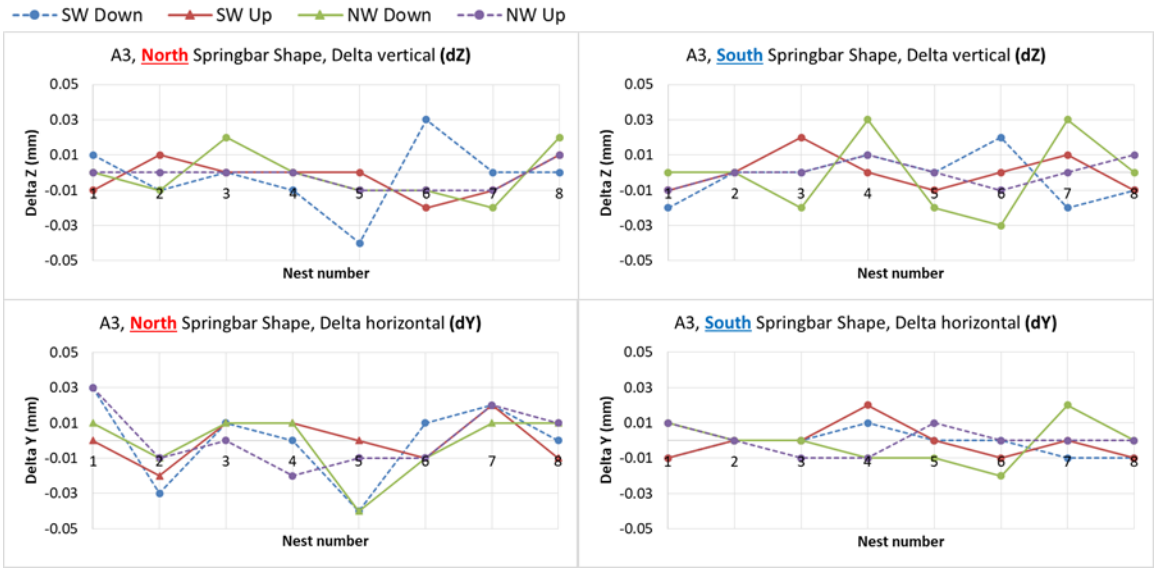

FIGURE 6-5: A3 springbar straightness; North springbar Delta Z,Y (top and bottom left), South springbar Delta Z,Y (top and bottom right)

6.2.4. Springbar orientation

Springbar orientation was evaluated to measure the change in relative position between the North and South springbars directly. The analysis was performed by calculating the changes in the coordinates for each drift nest relative to the Frame CS.

This analysis was similar to springbar planarity, but is provided here for completeness. The coordinates in the nominal were subtracted from the coordinates of each support condition. In this manner, changes in the relative position of each drift nest could be quantified as a result of a jack adjustment.

$$Delta\ Z,Y = Nest_{[e.g.\ SW\ down]} - Nest_{Nominal} \qquad \text{Equation 3}$$

Where,

$Nest_{[e.g.\ SW\ down]}$ are the Z and Y coordinates of single points after a jack adjustment, $Nest_{Nominal}$ are the Z and Y coordinates of single points in the nominal support condition, and $Delta\ Z,Y$ are the Z and Y differences in coordinates, respectively.

Note, that the above calculation is different than that for springbar straightness. Springbar straightness calculates the difference in point deviations to fitted lines. Springbar orientation calculates the change in the relative coordinates of each drift nest. The $Delta\ Z$ and $Delta\ Y$ values are graphed in FIGURE 6-6 and FIGURE 6-7 for the NE and NW jack relieved support conditions. The figures have different legends specific to the each jack adjustment. The North and South springbars are plotted in red and blue, respectively.

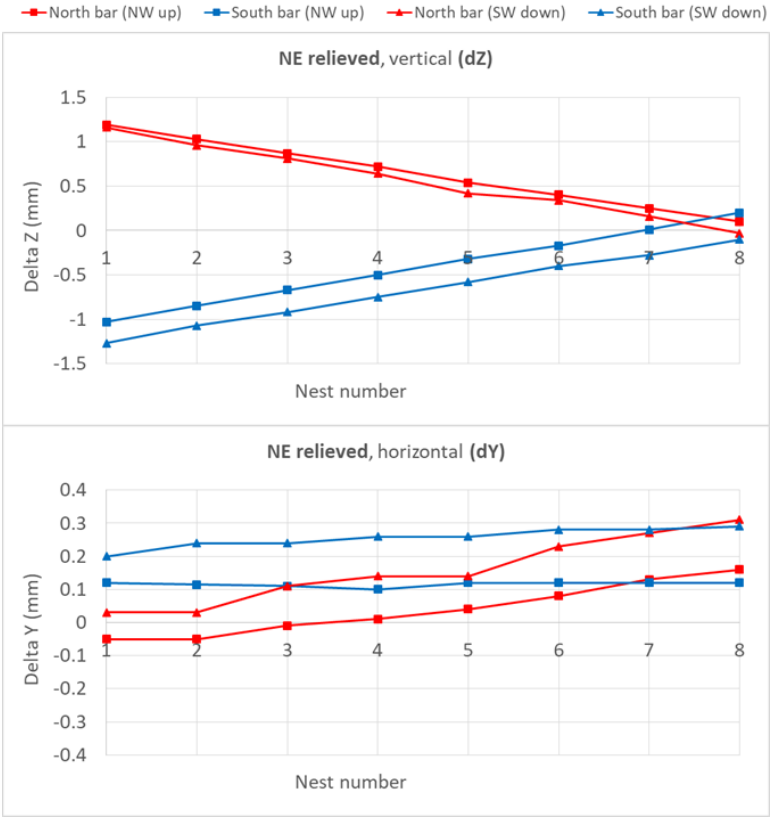

FIGURE 6-6: NE relieved, springbar drift nest coordinate changes relative to nominal

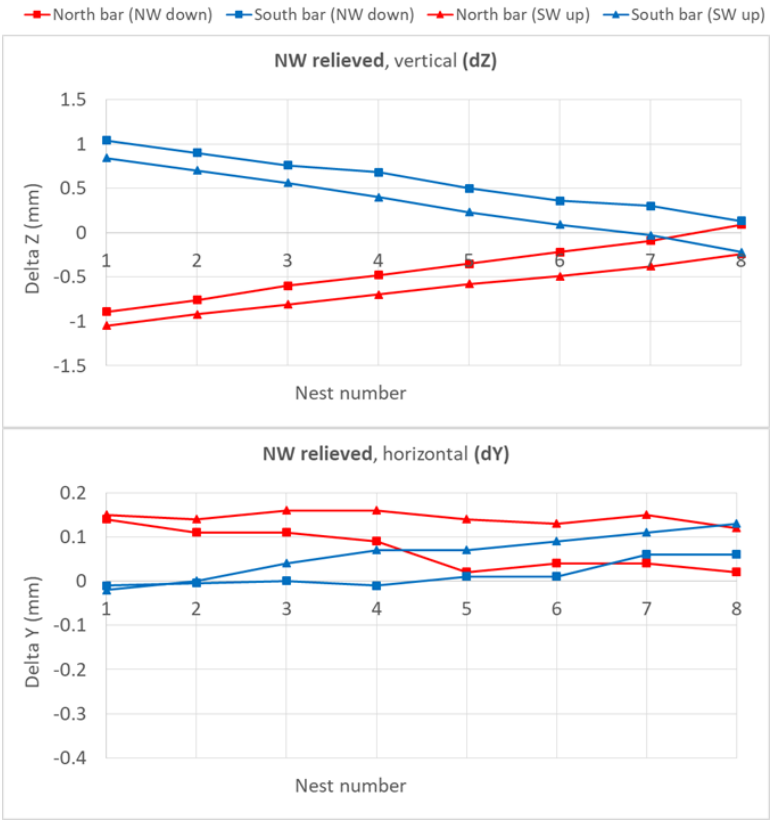

FIGURE 6-7: NW relieved, springbar drift nest coordinate changes relative to nominal

If the springbars were affected by torsion through the Frame due to a relieved jack, changes in their planarity would be visible by changes in the drift nest coordinates. In both support conditions, the Z coordinates were calculated to deviate nearly 1.5 mm from their nominal position. The angles between the springbar lines in the Z direction indicate a change in springbar orientation. While some changes in the Y direction were measured, they were not significant.

6.2.5. Finite element analysis

A finite element analysis (FEA) was conducted to observe theoretical deflections of a Model 1 generator Frame in the specific supporting conditions of the A3 rigid body experiment. FEA used a simplified CAD model of the A3 Frame, in which non-critical

features were removed. The Frame was assumed to be steel, with a mass of about 40,000 kg. The simulation software was NX 11 Pre-Post Application. A 100 mm tetrahedral mesh was created resulting in 156,750 elements. The analysis was performed by another student and is provided in the thesis for completeness.

To replicate the physical Cbeam jacks, constraints were placed on the modeled Frame at approximately the same locations. A fixed constraint was placed at the SW jack on the Frame while simply supported constraints, restricting only vertical motion, were placed at the remaining jacks. Gravity of 9.81 m/s^2 was the only applied force.

To replicate the jack adjustments from the experiment in FEA, either the NE or NW simply supported constraints were removed from the Frame. The FEA simulated the NE jack relieved and NW jack relieved supporting conditions. The nominal support condition was simulated with all fours jacks. Deflections were calculated as displacements from the ideal CAD model under no load.

The results of the nominal FEA deflections are shown in FIGURE 6-8, viewing the North springbar from the NLE. In this support condition, displacements throughout the Frame did not exceed 0.275 mm and were deemed negligible. Neither the BC distortion nor the springbars changed significantly from the CAD model.

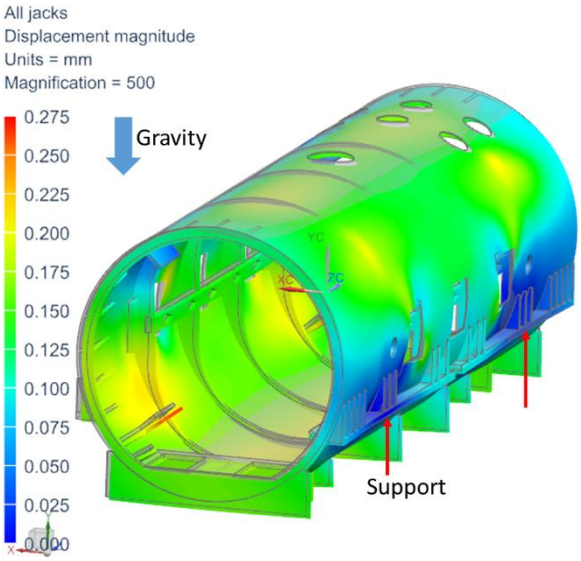

FIGURE 6-8: All jacks support condition, nominal FEA deflection viewing NLE

FEA results for the NE jack relieved and NW jack relieved supporting conditions are shown in FIGURE 6-9 and FIGURE 6-10. In both cases the BCs distorted to elliptical shapes, where the NLE and LE assumed alternating angles of twist. When the NE jack was relieved, the LE twisted towards the NE corner. When the NW jack was relieved, the NLE twisted towards the NW corner.

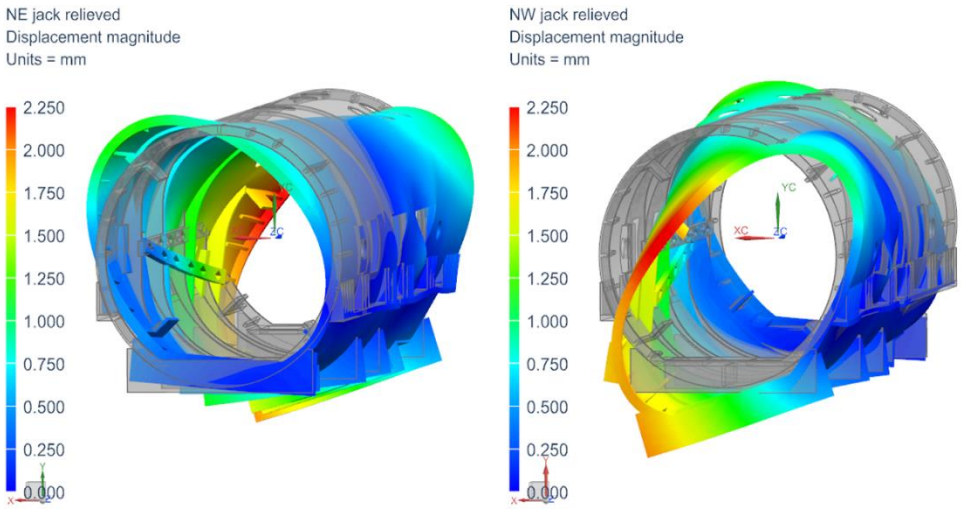

FIGURE 6-9: NE (left) and NW (right) relieve support condition FEA deflections, viewed from the NLE towards the north springbar, 500x magnification

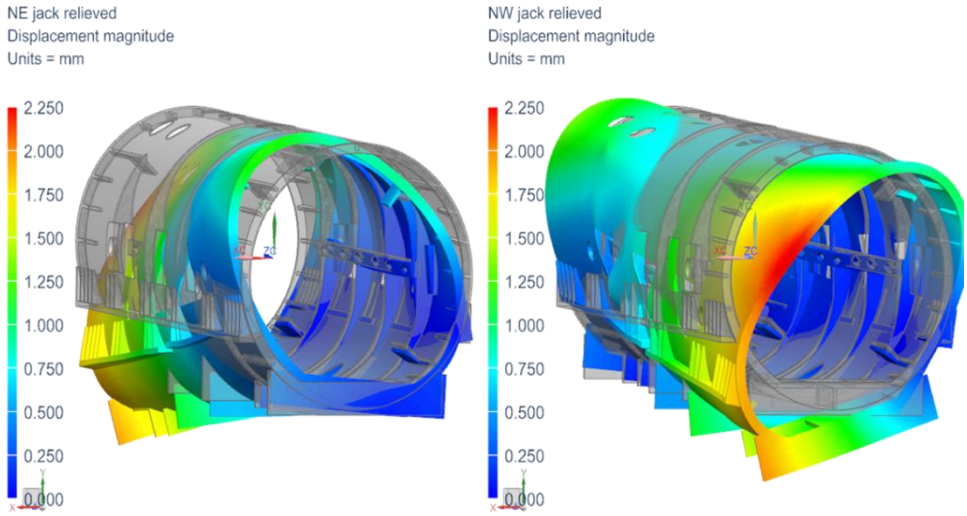

FIGURE 6-10: NE (left) and NW (right) relieved support condition FEA deflections, viewed from NLE towards south springbar, 500x magnification

The resulting springbar planarity values are presented in TABLE 6-2**.** Springbar planarity was evaluated by lines along the top inside edges of the springbars. A plane was fit to the NW, SW, and SE endpoints of the lines. The magnitude of the distance of the NE endpoint to the fitted plane was used as the measure of springbar planarity, similar to Section 6.2.1 and FIGURE 6-2.

TABLE 6-2: FEA springbar planarity deviation results

Support condition	Planarity deviation of NE endpoint (mm)	Total displacement (mm)
NE jack relieved	-1.77	3.53
NW jack relieved	1.77	

Due to symmetry, both support conditions produced a planarity deviation of ±1.77 mm. This resulted in a total displacement of 3.53 mm. Compared to the 4.22 mm total displacement from the experimental data, the experimental and FEA results agreed within 20%. Therefore, the FEA confirmed the springbar planarity changes measured in the experiment.

6.2.6. Rigid body takeaways and mitigation

In summary of the A3 rigid body experiment and FEA, several key takeaways were identified that impact the Core to Frame assembly process.

1. Experimental results were confirmed through FEA analysis.
2. Model 1 Frames changed shape depending on their support condition. For example, if a Frame was supported on its ribs on the shop floor, its BCs and springbars will be in different shapes when it is on the Cbeam jacks.
3. Predicted shim dimensions were guaranteed to be different than the ordered dimensions if the predictions were based on measurements obtain in a different support condition.
4. To achieve an untwisted alignment using the proposed process, the Frame must be in an untwisted state during measurement.

5. Pre-manufactured shims would “force” the Frame into the twist condition present during its measurement.

By implementing a mitigation strategy, a repeatable support condition could be created for the Frame during its measurement. This would support the Frame in a desirable shape and improve the measurements. These mitigation strategies were suggested to the manufacturer for implementation and are presented in TABLE 6-3. Each mitigation strategy is presented with its major advantage (Pro) and disadvantage (Con).

TABLE 6-3: Frame rigid body mitigation strategies

Frame measurement method	Pro	Con
1) Measure on Cbeam	Equal pressure lift untwists Frame.	Cbeam use; complicates measurement.
2) Measure on custom rib support stand	Frame untwisted on ribs; no Cbeam.	Requires floor space, money.
3) Disregard twist	Simple.	Accept twisted Frame.
4) Measure on parallels	Frame untwisted on parallels; no Cbeam.	Requires parallels.
5) Numerical compensation	No physical mitigation.	Requires confident characterization of Frames

The first strategy would use existing equipment. However, performing an Equal Pressure Lift would complicate the procedure and extend the time spent at the Cbeam station. The second strategy would require a new set up, where small, adjustable jacks would be placed underneath the Frame ribs while on the shop floor. This set up would put the Frame in an untwisted state, but require additional costs and floor space.

FEA was performed to assess the second mitigation by examining the change in shape of a Model 1 Frame when supported under the ribs versus at the Cbeam jack

locations. The analysis was performed by another student and is provided for completeness. The resulting distortion is shown in FIGURE 6-11. Deflections were purely vertical in the FEA. The NLE BC distorted to a roundness of about 1.5 mm, significantly different than when supported at the Cbeam jack locations. The strategy was determined not ideal for a Model 1 generator.

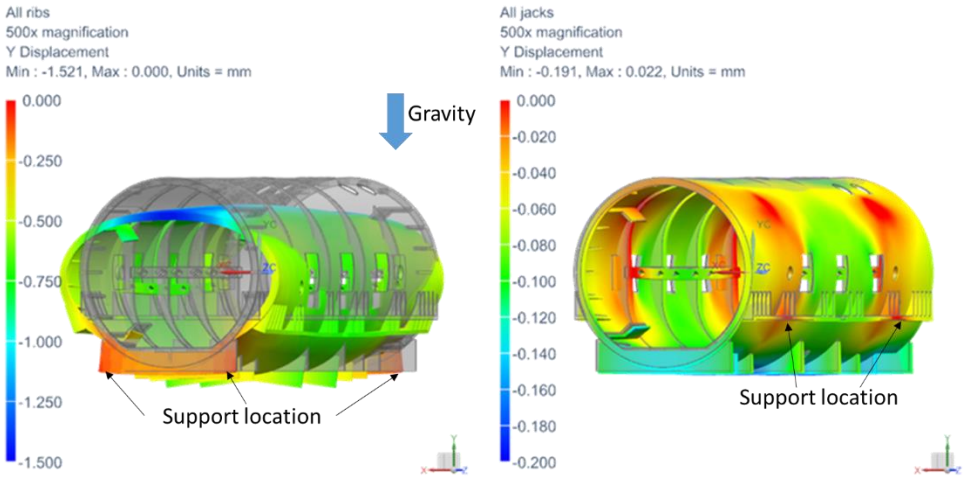

FIGURE 6-11: FEA deflections for all ribs (left) and all jacks (right), viewing NLE, 500x magnification

The third mitigation strategy is the simplest approach. If the alignment tolerances of the Core and Frame are large enough to make the rigidity effects of the Frame negligible, no mitigation would be needed. However, the manufacturer's engineering team would need to verify this approach.

In the fourth strategy, a Frame would be untwisted if supported by parallels, as shown in FIGURE 5-6 for Generator A3. The untwisted state would be achieved without the use of the Cbeam station, but would require shop floor space and a set of parallels.

The fifth mitigation strategy is similar to the third, in that no physical mitigation would be necessary. Rather, a numerical compensation would be developed to compensate for observed deflections in the Frame's shape. The Frame could be

measured in any support condition and numerical compensation could be applied to the shim calculation procedure. This strategy was not evaluated, and additional work is needed to determine its feasibility and accuracy.

CHAPTER 7. MODEL 2 DIGITAL ASSEMBLY RESULTS

Following measurements of the Model 1 generators, the manufacturer introduced the Model 2 generator. The Model 2 was more versatile and suitable for a variety of generation needs, and featured a Frame with increased stiffness. The introduction of the Model 2 was not a result of the project and its findings. Nevertheless, two Model 2 generator Frames and Cores were measured and analyzed using the proposed process. The shim results, Case C alignments, BC deformations, and rigid body experimentation were evaluated.

7.1. Model 2 shim results

The shim results, based on Case B alignments, for the Model 2 are presented in TABLE 7-1, listing the same information as in TABLE 5-1. The complete table of shim differences is provided in APPENDIX B.

TABLE 7-1: Shim results for Model 2 generators

Generator	Support	Date	Shim: Case B Predicted - Ordered (mm)		Gap: Case B Predicted - Ordered (mm)	
			Max.	Avg. (abs)	Max.	Avg. (abs)
A5	Cbeam jacks	September 2017	0.52	0.28	0.17	0.07
A6	Ribs on plastic	November 2017	0.65	0.29	0.20	0.05

Predicted shims of the two Model 2 generators revealed fairly consistent values with the ordered shims. While the differences between the dimensions were not expected to be zero, the improved stiffness of the Frame did mitigate some of the previously observed rigidity issues. The absolute average was 0.28 mm and 0.29 mm for A5 and

A6, respectively. These low averages indicated that Frames maintained a consistent shape between measurements made on the shop floor and when they are made on the Cbeam jacks. Although the maximum differences were 0.52 mm and 0.65 mm for the generators, this did not mean that the predicted shims, if used in physical assembly, would be unable to produce an in tolerance alignment.

The absolute averages for the total gaps were minimal, being 0.07 mm and 0.05 mm for A5 and A6, respectively. This confirmed that the local component geometries were characterized correctly and that relative orientation of the Frame and Core was the main source of variation in the shim differences.

7.2. Model 2 Case C results

Case C digital alignment was performed for each Model 2 generator, following the description in Section 5.2. The resulting shim differences are presented in FIGURE 7-1. The vertical axis “Case C Predicted – Ordered (mm)” indicates differences in the shim dimensions between those calculated in digital Case C alignment and those measured after the contractor aligned the physical components.

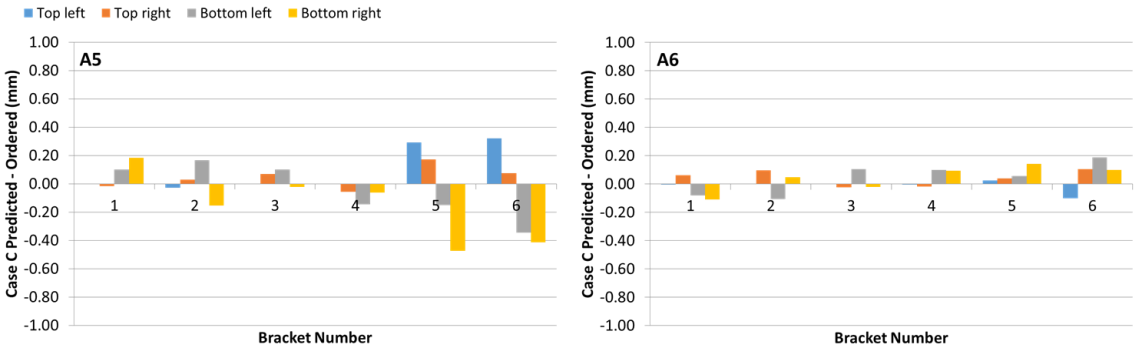

FIGURE 7-1: A5 (left) and A6 (right) Model 2 Case C shim results

For both generators, the largest shim difference was less than 0.50 mm. While a slope in shim differences from B4 to B6 is slightly noticeable for Generator A5, the total magnitudes are much less than those observed in the Model 1 Case C results. No sloping trend is observable in the shim differences from B4 to B6 for Generator A6. Therefore, no significant changes in the orientations of the springbars were found, reinforcing the increased stiffness of the Model 2 design.

7.3. Model 2 bolt circles

Similar to the Model 1 BC analysis described in Section 5.4, the Model 2 Frame BCs were evaluated in SA. An ellipse was unable to be fit to any of the BCs due to their minimal circularity deviations. The BC data is shown in FIGURE 7-2.

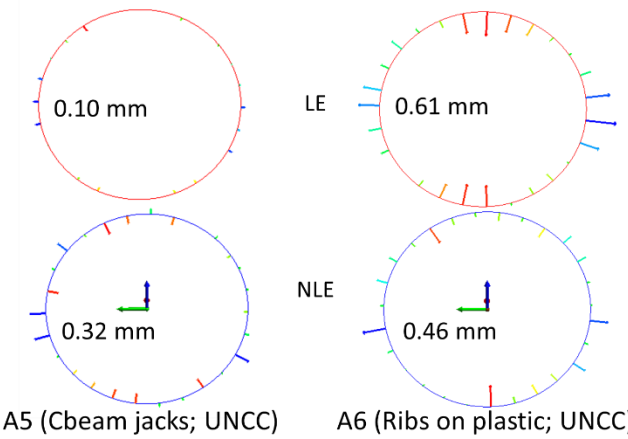

FIGURE 7-2: A5 and A6 bolt circle roundness, no ellipticity, (1000x vector magnification)

Generator A5 was calculated to have a maximum roundness of 0.10 mm and 0.32 mm for its NLE and LE BCs, respectively. Generator A6 had a roundness of 0.61 mm and 0.46 mm for its NLE and LE BCs, respectively. These low deviations did not distort the BCs into approximate elliptical shapes. Compared to the roundness values of the Model 1 generators, ranging from 1.1 mm to 2.1 mm, the Model 2 BCs were significantly more circular.

In conclusion, the increased stiffness of the Model 2 Frame reduced variations in the shim results for both Case B and Case C alignments. The BCs were not distorted into elliptic shapes, implying that the effect of the model 2 Frame's support condition was greatly reduced.

7.4. Model 2 rigid body experiment

The A3 rigid body experiment was simplified and replicated for the Model 2, A5 Frame. Instead of using 8 drift nests along the springbars, the threaded holes for the yaw bolts at each bracket location were measured with the SMR. Single data points were measured at B1, B3, B4, and B6 locations. These points were labeled to the

corresponding corners of the Frame. The locations of these points relative to the first and last drift nests on the Model 1 experiment springbars were close enough to be a good representation of the endpoints.

The points were measured with the Frame on the Cbeam in three support conditions: nominal, SW jack relieved, and NW jack relieved. An Equal Pressure Lift was performed for the nominal condition. Springbar planarity was analyzed similar to FIGURE 6-2, however using the measured points at the threaded holes rather than the endpoints of fitted lines. The B6 measured point represented the NE endpoint.

TABLE 7-2 presents the results of the experiment, where the nominal planarity value was subtracted from the two other support conditions. After relieving the SW jack, the NE endpoint (B6) was found to deviate -0.32 mm below springbar plane. When the NW jack was relieved, the NE endpoint deviated 1.02 mm above the plane. The total displacement of the NE endpoint between the two support conditions was 1.34 mm.

TABLE 7-2: A5 Experimental springbar planarity deviation results

Support condition	Jack adjustment	Planarity deviation of NE endpoint (mm)	Total displacement (mm)
SW jack relieved	NW up	-0.32	1.34
NW jack relieved	NW down	1.02	

Recalling the A3 rigid body experiment planarity values, its total displacement was 4.22 mm between the support conditions. Using total planarity displacement as a ratio of stiffness, the Model 2 Frame was found to be about 3 times stiffer than the Model 1. This value was calculated by dividing 4.22 mm by 1.34 mm.

The stiffness ratio indicated that the Model 2 Frames may be sufficiently rigid to neglect the support condition. If this was true, the Frame could be supported in any

reasonable support condition, resulting in negligible effects to the predicted shim dimensions.

CHAPTER 8. CBEAM ALIGNMENT AND RESULTS

To validate the proposed process and methodology, two assembly tests were performed using premanufactured shims of the Model 2 generators. To predict shims the Frame and Core were digitally assembled in Case A alignments. Only four top shims at B1, B3, B4, and B6 were fabricated. The shims were manufactured on a 3-axis milling machine at UNCC. Any tapers across the shims were achieved by placing feeler gages underneath them.

The assembly test using premanufactured shims is listed below. Recall FIGURE 3-2 for the generator alignment nomenclature.

1. The Frame and Core were placed on the Cbeam.
2. The Frame was shifted along X to meet the axial alignment.
3. The Frame was adjusted along Y using the yaw bolts and the horizontal alignment was set using yaw blocks at B1 and B3. Yaw blocks were small blocks used to fill the horizontal gaps B1 and B3, as illustrated in FIGURE 8-1. The yaw bolts remained tightened to maintain the Core's position.
4. Top shims at B1, B3, B4, and B6 were placed into assembly, constraining the Z, pitch, and roll dimensions.
5. The contractor verified the alignment using their method.

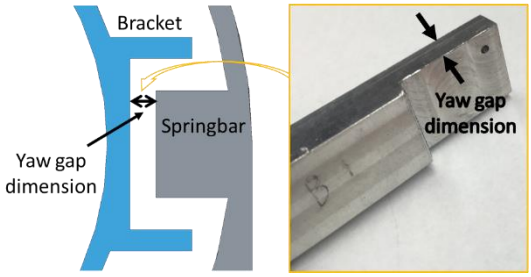

FIGURE 8-1: Yaw gap between a bracket and springbar (left); machined yaw block (right)

The shims were placed into assembly following a procedure referred to as Down and Up after the Frame had been axially aligned to the Core on the Cbeam. The Frame was lowered and the shims were placed onto the springbars in their respective locations. The Frame was then raised until the shims made full contact with the brackets. Down and Up is illustrated in FIGURE 8-2.

After the yaw blocks and shims had been placed, the contractor performed a verification measurement to evaluate the achieved alignment.

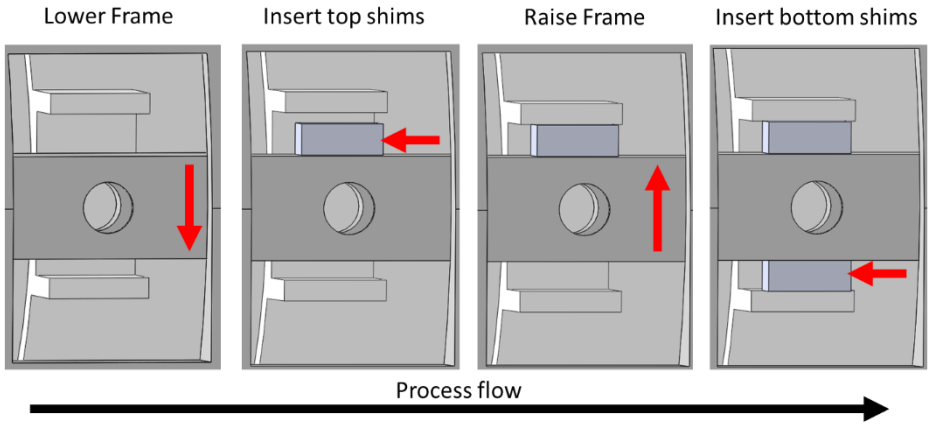

FIGURE 8-2: Down and Up shim placement; step 4 of alignment with pre-manufactured shims

8.1. A5 Cbeam alignment test

The first test was performed on the Model 2, A5 generator. As a mitigation strategy, the Frame was measured on the Cbeam, after an Equal Pressure Lift, with a reference network around the station. The alignment tolerance on all five dimensions

(excluding axial) was ±0.8 mm. The achieved alignment values as compared to the nominal are presented in TABLE 8-1. Roll was determined by Z coordinates of the North and South clocking points relative to the Core CS. Half the difference between the Z components determined roll.

The test concluded with 4 out of 5 dimensions in tolerance. All dimensions controlled by the shims were within their tolerance, those being NLE Z, LE Z, and roll. The NLE Y dimension was nearly out of tolerance and the LE Y exceeded the tolerance.

TABLE 8-1: A5 alignment test results, represented in Core CS (±0.8 mm tolerance)

Dimension	Achieved (mm)	Nominal (mm)	Deviation (mm) (Ach - Nom)
NLE bolt circle Y	-0.74	0.00	-0.74
NLE bolt circle Z	0.79	0.61	0.18
LE bolt circle Y	1.55	0.00	1.55
LE bolt circle Z	0.76	0.66	0.10
Roll: (North clocking Z - South clocking Z)/2	0.28	0.00	0.28

The A5 test results showed that the proposed methodology using premanufactured shims was capable of producing an in-tolerance alignment. However, for this test, the yaw gaps were incorrectly calculated and no yaw blocks were used to set the horizontal alignment. Additionally, after step 3 the yaw bolts were loosened, causing the Core to roll on the Cbeam and the horizontal alignment to change before step 4. These issues were remedied in the Generator A6 test.

8.2. A6 Cbeam alignment test

Due to time constraints, the A6 Frame was measured with its ribs on plastic sheets. Because the Frame BCs were measured to have minimal roundness errors, the

Frame was assumed to be sufficiently untwisted. In the test procedure, the yaw bolts were left in their tightened positions during shim placement.

The test concluded with all alignment dimensions in tolerance, with the largest deviation being 0.53 mm for the LE BC Z coordinate. The completion of the test was a successful demonstration of the proposed process. The proposed process was proven capable of producing in tolerance alignments.

TABLE 8-2: A6 alignment test results, represented in Core CS (±0.8 mm tolerance)

Dimension	Achieved (mm)	Nominal (mm)	Deviation (mm) (Ach - Nom)
NLE BC Y	-0.10	0.00	-0.10
NLE BC Z	0.43	0.61	-0.18
LE BC Y	0.18	0.00	0.18
LE BC Z	1.19	0.66	0.53
Roll: (North clocking Z - South clocking Z)/2	0.33	0.00	0.33

CHAPTER 9. MEASUREMENT EVALUATION

No single uncertainties were stated for the measurements made throughout the project in the proposed process or for the Model 2 Cbeam alignment tests. However, some metrics were used for creating a basic idea of the measurement quality.

The manufacturer's literature of the laser tracker typically used for the proposed process measurements stated a radial maximum permissible error (MPE) of 16 μm + 0.8 μm/m in absolute distance measurement (AMD) mode and an angular MPE of 20 μm + 5 μm/m. The MPE values were specified per ASME B89.4.19-2006 [22] . Following the *GUM* [23] the radial and two angular uncertainties were calculated based on uniform distributions of the MPEs at 10 m. The combined standard uncertainty was calculated with uncorrelated uncertainties to a first order approximation, using sensitivity coefficients of one. The expanded uncertainty was obtained by multiplying the combined standard uncertainty by a coverage factor of 2 (k=2) and calculated to be 118 μm at 10 m. Most measurements for the proposed processes ranged between 5 m and 16 m.

For understanding repeatability of the proposed process measurements, the locations of the reference points were measured twice from each tracker position. The reference points were measured before and after the component features were measured at each tracker position. The reference point displacements (RPDs) are the differences in coordinates of individual reference points between their first and second measurement in the tracker's CS. These differences may have been caused by a displacement in the tracker position, a displacement in drift nests, or weather and mechanical changes in the

environment or tracker that would have occurred during the measurement of a component.

The maximum and RMS values are provided in TABLE 9-1 for the Generator A4 Core as an example. The complete table of generator RPD differences is provided in APPENDIX C. If the maximum RPD difference from a single tracker position was greater than 0.2 mm, the cause was identified and the measurements were retaken. In practice, some measurements were not retaken due to time constraints.

For the Generator A4 Core, from the LE North Brackets instrument position (tracker position 1 in FIGURE 4-13), the maximum RPD was 0.212 mm. The cause was identified as a railroad car moving through the shop floor. A typical measurement duration at a single instrument position was 30 minutes. During this time, the railroad car moved, causing deformations in the shop floor and the drift nests to be displaced.

TABLE 9-1: A4 Core RPD differences

Generator	Support condition	Instrument Position	Max (mm)	RMS (mm)	Cause
A4 Core	v-blocks	LE North brackets	0.212	0.159	Rail road car moved during measurement
		LE North brackets redo	0.074	0.040	
		LE center	0.070	0.040	
		LE South brackets	0.094	0.056	

Another example of RPDs was the measurement of the Generator A5 Frame on the Cbeam. During measurements from the NLE tracker position, a neighboring generator was lifted by a gantry crane and moved to another location. After checking the reference points, the movement caused a maximum RPD of 1.161 mm, almost entirely in the vertical direction, as illustrated in FIGURE 9-1. Moving the neighboring generator

caused the shop floor to deform, thereby displacing the drift nests from their original locations.

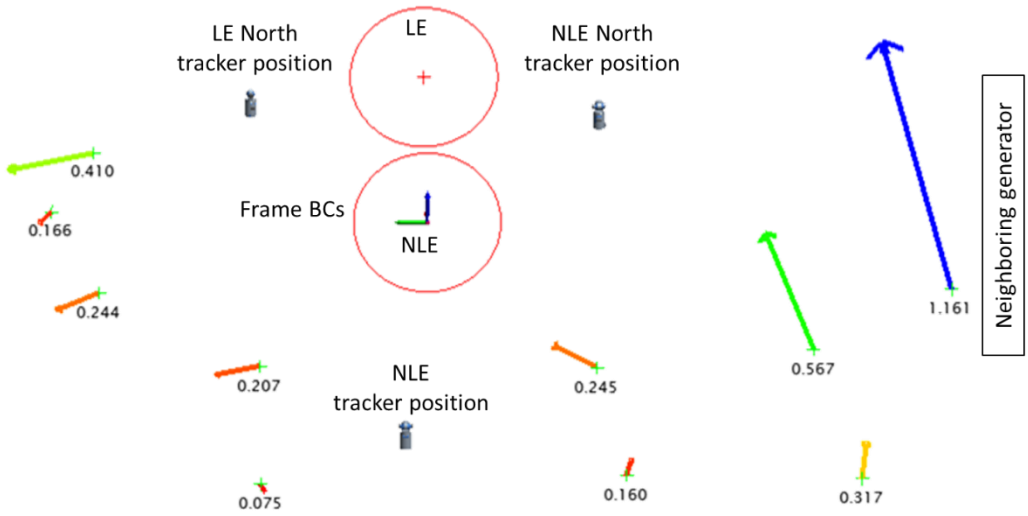

FIGURE 9-1: RPD differences during measurement of A5 Frame on the Cbeam, 500x vector mag.

Defining the measurement quality for shim predictions and the generator alignments using premanufactured shims was a complicated task. However, the above analysis gives a basis for understanding how the variations in the shop environment may have influenced the measurements. Quantifying all of the influencing factors in the shop environment would be a difficult task. Additionally, measuring weather changes using an established network of sensors throughout the measurement volume was impractical.

CHAPTER 10. CONCLUSION

The project has shown that digital assembly based on as-built component measurements can be used for part dimensioning and predictive shimming to improve large scale manufacturing processes. The methodology was applied to the assembly of power plant generators and successfully demonstrated its feasibility in reducing costs, improving product quality, and increasing productivity. Measurements were made using a laser tracker on six generators and shim dimensions were calculated, then compared to those from the current process. The study revealed that it is important to understand the effects of a component's support condition on its shape and to identify and reduce the effects of a dynamic shop environment on measurement accuracy.

To further implement this methodology into the generator assembly, additional work may be necessary to validate and quantify the relationship between the Frame support condition and shape. The large component is susceptible to deformations due to gravity which may govern its alignment to the Stator Core and potentially lead to issues, such as a decrease in generator efficiency. Therefore, it is necessary to define a repeatable support condition for the Frame when it is measured. Additionally, both the Frame and Stator Core measurement setups should be isolated from activities in the surrounding shop environment.

To utilize digital assembly for other large scale applications like predictive shimming, several challenges must be addressed. These are, choosing component measurands necessary to define local coordinates systems and perform shim calculation, setting up a laser tracker and reference network to acquire all the measurements,

quantifying the effects of a component's support condition on its shape, minimizing the effects of shop activities during measurement, evaluating measurement uncertainty, and comparing the methodology to existing processes.

CHAPTER 11. FUTURE WORK

Work for the immediate future may be related to the evaluation of non-rigid body effects in large objects and any subsequent mechanical or numerical compensations applicable to coordinate metrology and large scale manufacturing. A quantified relationship between gravitational sag in large components may prove useful to many manufacturers.

Additionally, work could be done to evaluate the measurement uncertainty in the thesis project's application. Environmental factors could be identified, quantified, and related to the measurements and alignments. A method could be proposed for practically measuring the weather changes in a dynamic measurement space. The effect of tying multiple laser tracker positions together across large areas in an active shop environment could also be studied.

The methodology of utilizing digital assembly could also be explored for alternative applications such as predictive machining operations for seal plates used in rotor assembly and tool path planning for the final machining of castings and weldments. Effort can be made in the application of closed loop metrology systems to develop virtual twin data structures for inspection, analysis, or manufacturing.

REFERENCES

[1] Estler, W.T., Edmundson, K.L., Peggs, G.N., Parker,D.H. "Large-Scale Metrology – An Update." NIST, NPL, NRAO.

[2] Goch, G. Knapp, W., Hartig, F. (2012) "Precision Engineering for Wind Energy Systems." CIRP Annals – Manufacturing Technology.

[3] Schmitt, R.H., et al. "Advances in Large-Scale Metrology – Review and future trends." CIRP Annals – Manufacturing Technology, 2016.

[4] Kayani, A., Maropoulos, P., Martin, O., Muelaner, J. "Measurement Assisted Assembly and the Roadmap to Part-to-Part Assembly." 7th International Conference on Digital Engerprise Technology, DET 2011.

[5] Maropoulos, P.G., Martin, O.C., Muelaner, J.E. "Achieving Low Cost and High Quality Aero Structure Assembly through Integrated Digital Metrology Systems." Forty Sixth CIRP Conference on Manufacturing Systems, CIRP 2013.

[6] Cai, B., Maropoulos, P.G., Muelaner, J.E. "Large Volume Metrology Instrument Selection and Measurability Analysis." Department of Mechanicla Engineering, The University of Bath, Bath, UK.

[7] Cai, B., Guo, Y., Jamshidi, J., Maropoulos, P.G. "Large volume metrology process models: A framework for integrating measurement with assembly planning." CIRP Annals Manufacturing Technology, 2008.

[8] Permin, E., et al. "Self-optimizing production systems." 48th CIRP Conference on Manufacturing Systems, CMS 2015.

[9] Witte, A., Schmitt, R., JanBen, M. Bertelsmeier, F. "Metrology assisted assembly of airplane structure elements." Conference on Assembly Technologies and Systems, CIRP, 2014.

[10] Blaedel, K., et al. "Metrology of Non-Rigid Objects." LLNL. January 1, 2002.

[11] Maropoulos, P. G., Muelaner, J.E. "Large Volume Metrology Technologies for the Light Controlled Factory." 8th International Conference on Digital Enterprise Technology – DET 2014, CIRP, 2014.

[12] Cuypers, W., et al. "Optical measurement techniques for mobile and large-scale dimensional metrology." Optics and Lasers in Engineering. 2009.

[13] Sawyer, D., Muralikrishnan, B., Phillips, S. "Laser trackers for large-scale dimensional metrology: A review." NIST. Presidion Engineering, 2016.

[14] Kunsmann, H., et al. "Productive Metrology – Adding Value to Manufacture."

[15] Savio, E., De Chiffre, L., Carmignato, S., Meinertz, J. "Economic benefits of metrology in manufacturing." CIRP Annals – Manufacturing Technology, 2016.

[16] Smith, S. "The Need Research and Development in Manufacturing and Metrology." Critical National Need Idea. The University of North Carolina at Charlotte.

[17] Erdem, I., et al. "A novel comparative design procedure for reconfigurable assembly fixtures." CIRP Journal of Manufacturing Science and Technology. 2017.

[18] Fuzhou, Du., Zhehan, C., Xiaoqing, T. "Research on uncertainty in measurement assisted alignment in aircraft assembly." Chinese Society of Aeronautics and Astronautics & Beihang University, Chinese Journal of Aeronautics, 2013.

[19] Galetto, M., et al. "Uncertainty evaluation of distributed Large-Scale-Metrology systems by a Monte Carlo approach." CIRP Annals – Manufacturing Technology, 2016.

[20] Wang, Q., Zissler, N., Holden, R. "Evaluate error sources and uncertainty in large scale measurement systems." Robotics and Computer-Integrated Manufacturing, 2013.

[21] Calkins, J.M., Salerno, R.J. "A Practical Method for Evaluating Measurement System Uncertainty." New River Kinematics. 2000 Boeing Large Scale Metrology Conference.

[22] ASME B89.4.19-2006. "Performance Evaluation of Laser-Based Spherical Coordinate Measurement Systems."

[23] "JCGM 100:2008 – Evaluation of Measurement Data – Guide to the Expression of Uncertainty in Measurement." BIPM, 2008.

APPENDIX A. CIRCLE FITTING ALGORTIHM

BC_circle.m

```
%Michael Erickson
%CIRCLE
%This function fits a circle to (x,y) point data using the general
formula
%for least squares, linearized for a well traced line.

%Open the file of points.  This assumes the points are in [x,y] format.
clear all; close all; clc;
filename = ('yz.boltholes.txt');
file_id = fopen(filename, 'r');
pts = fscanf(file_id, '%g %g' ,[2,inf]);
fclose(file_id);

%%%%%
%Plot all 128 bolt holes
figure(1);
pts = pts';
num = 'All';
[Ro1, xo1, yo1] = circleFit(pts);
plotCircle( Ro1, xo1, yo1, num ); hold off;

%%% 3rd
%Plot all every 3rd bolt holes
figure(2);
n = 3;
num = 'Every 3rd';
ptsx = pts(:,1); ptsy = pts(:,2);
p3x = ptsx(2:n:end-1);
p3y = ptsy(2:n:end-1);
pts3=[p3x p3y];

[Ro3, xo3, yo3] = circleFit(pts3);
plotCircle( Ro3, xo3, yo3, num );

%%% 5th
%Plot all every 5th bolt holes
figure(3);
n = 5;
num = 'Every 5th';
ptsx = pts(:,1); ptsy = pts(:,2);
p5x = ptsx(2:n:end-2);
p5y = ptsy(2:n:end-2);
pts5=[p5x p5y];

[Ro5, xo5, yo5] = circleFit(pts5);
plotCircle( Ro5, xo5, yo5, num );

%%% 7th
```

```
%Plot all every 7th bolt holes
figure(4);
n = 7;
num = 'Every 7th';
ptsx = pts(:,1); ptsy = pts(:,2);
p7x = ptsx(2:n:end-1);
p7y = ptsy(2:n:end-1);
pts7=[p7x p7y];

[Ro7, xo7, yo7] = circleFit(pts7);
plotCircle( Ro7, xo7, yo7, num );

%%% 9th
%Plot all every 7th bolt holes
figure(5);
n = 9;
num = 'Every 9th';
ptsx = pts(:,1); ptsy = pts(:,2);
p9x = ptsx(2:n:end-1);
p9y = ptsy(2:n:end-1);
pts9=[p9x p9y];

[Ro9, xo9, yo9] = circleFit(pts9);
plotCircle( Ro9, xo9, yo9, num );
%%%%%%%%%
%set(gca,'fontsize','14');
figure(6);
X = [xo1; xo3; xo5; xo7; xo9];
Y = [yo1; yo3; yo5; yo7; yo9];
plot(X,Y,'k+');
xlabel('Y [mm]'); ylabel('Z [mm]');
xlim([-0.1 0.1]); ylim([-0.05 0.05]);
m = 0.0025*2;
text(xo1,yo1+m,'All');
text(xo3-m/2,yo3+m,'3rd');
text(xo5,yo5+m,'5th');
text(xo7+m,yo7,'7th');
text(xo9,yo9+m,'9th');
```

circleFit.m

```
function [ Ro xo yo ] = circleFit( pts )
%Input X,Y point data. Output Radius (Ro), circle center (xo,yo).

%Extract the column data into unique arrays.
n = length(pts);        %Number of points
x = pts(:,1);           %x coordinates
y = pts(:,2);           %y coordinates
%Calculate the initial incremental guess.
xinc = mean(x);
yinc = mean(y);
xo = xinc;
```

```
yo = yinc;
crit = 0.00001;
counter = 0;
%Fit a circle using Least Squares general method.
while abs(xinc) > crit && abs(yinc) > crit
    counter = counter + 1;

    xnew = x-xo;  %X coordinate in new CS
    ynew = y-yo;  %Y coordinate in new CS

    r = (xnew.^2 + ynew.^2).^(1/2); %Calculate radius of each point to
center.
    theta = atan2(ynew,xnew);       %Calculate theta of each point to
center.

    c = cos(theta);          %Prepare variables for matrix.
    s = sin(theta);          %Prepare variables for matrix.

    A1 = [c,s,ones(n,1)];    %first A matrix
    b1 = r;                  %first b matrix

    A = A1'*A1;              %A matrix
    b = A1'*b1;              %b matrix

    coefs = A\b;             %Solve system of equations
    xinc = coefs(1); yinc = coefs(2); Ro = coefs(3); %extract solution.

    xo = xo + xinc;     %Add solution origin (in new CS) to original CS
increment.
    yo = yo + yinc;     %Add solution origin (in new CS) to original CS
increment.
end
%Calculate residuals. Residuals are calculated in the new CS.
% residuals = r - Ro;
% devmax = max(residuals);
% devmin = min(residuals);
% mxr = find(residuals==devmax);
% mnr = find(residuals==devmin);
% xx = [x(mxr); x(mnr)]; yy = [y(mxr); y(mnr)];

end
```

plotCircle.m

```
function plotCircle( Ro, xo, yo, num )
%Input Radius (Ro), circle center (xo,yo). Output cricel plot

%Plot the original data in original CS and the fitted data in original
CS.
angle = 0:0.01:2*pi;
xfit = xo + Ro*cos(angle);
```

```
yfit = yo + Ro*sin(angle);
plot(xo,yo,'kx'); hold on; plot(xfit,yfit); axis equal;
xlabel = ('SAF'); ylabel('Y'); zlabel ('Z');
axis equal;

%Print solution.
disp(num)
disp('The solution values are:')
fprintf(' xo = %f\n yo = %f\n Ro = %f\n',xo,yo,Ro)

end
```

yz.boltholes.txt

Y	Z								
1768.498	-583.726	47.14509	-1859.17	-1735.37	-669.367	-1217.53	1408.94	915.5344	1617.348
1737.84	-669.689	-44.1288	-1859.14	-1766.4	-583.481	-1146.86	1466.793	993.9152	1570.445
1702.911	-754.145	-135.262	-1854.68	-1793.12	-496.121	-1073.56	1521.155	1069.837	1519.732
1663.92	-836.628	-226.165	-1845.71	-1815.58	-407.592	-997.578	1571.807	1143.279	1465.381
1620.895	-917.167	-316.238	-1832.3	-1833.58	-318.109	-919.026	1618.636	1213.912	1407.537
1573.89	-995.497	-405.98	-1814.43	-1847.18	-227.806	-838.4	1661.573	1281.64	1346.294
1523.08	-1071.41	-494.684	-1792.13	-1856.29	-136.927	-755.911	1700.546	1346.376	1281.798
1468.666	-1144.7	-582.047	-1765.6	-1861.03	-45.7471	-671.614	1735.471	1407.761	1214.233
1410.736	-1215.25	-667.892	-1734.85	-1861.19	45.61846	-585.493	1766.097	1465.774	1143.753
1349.415	-1282.88	-752.288	-1699.89	-1856.79	136.7703	-497.999	1792.506	1520.207	1070.528
1284.717	-1347.48	-834.799	-1660.82	-1848.05	227.6963	-409.51	1814.629	1571.123	994.6496
1217.194	-1408.69	-915.401	-1617.76	-1834.78	318.0032	-319.812	1832.352	1618.32	916.4186
1146.444	-1466.64	-993.934	-1570.73	-1817.11	407.6219	-229.487	1845.58	1661.557	835.9159
1072.977	-1520.95	-1069.59	-1520.12	-1795	496.1962	-138.516	1854.44	1700.696	753.511
996.9547	-1571.66	-1142.97	-1465.75	-1768.57	583.5588	-47.2868	1858.857	1735.867	669.1956
918.7426	-1618.54	-1213.62	-1407.75	-1737.97	669.5854	43.88186	1858.832	1766.598	583.2897
838.1959	-1661.48	-1281.17	-1346.56	-1703.14	754.0172	135.1901	1854.228	1793.315	495.99
755.6742	-1700.48	-1345.84	-1281.95	-1664.07	836.528	226.0685	1845.218	1815.736	407.4337
671.1145	-1735.34	-1407.15	-1214.36	-1621.18	917.2346	316.4518	1831.752	1833.912	317.8709
585.1262	-1766.06	-1465.22	-1143.8	-1574.13	995.4128	405.9498	1813.888	1847.416	227.6208
497.691	-1792.55	-1519.77	-1070.61	-1523.42	1071.374	494.6079	1791.636	1856.558	136.7535
409.2645	-1814.65	-1570.56	-994.763	-1468.9	1144.703	581.943	1765.127	1861.178	45.57149
319.552	-1832.45	-1617.74	-916.564	-1411.13	1215.304	667.9099	1734.357	1861.24	-45.7624
229.1462	-1845.77	-1661.04	-836.091	-1349.76	1283.017	752.3872	1699.406	1856.981	-136.95
138.3058	-1854.74	-1700.25	-753.689	-1285.19	1347.542	834.97	1660.38	1848.07	-227.868
								1834.92	-318.202
								1817.101	-407.654
								1795.016	-496.345

APPENDIX B. SHIM RESULTS

TABLE B-1: A1 (Model 1) shim results

		Ordered, for Cbeam alignment				Case B Predicted			
A1		Shims sizes		Total gap size		Shims: Case B Predicted - Ordered		Gap: Case B Predicted - Ordered	
Bracket		Left (mm)	Right (mm)	Left (mm)	Right (mm)	Left (mm)	Right (mm)	Left (mm)	Right (mm)
B1	Top	29.007	29.18	79.02	79.07	0.22	0.18	0.21	0.14
	Bottom	50.01	49.89			-0.01	-0.04		
B2	Top	30.56	30.28	78.92	78.87	-0.07	-0.13	-0.06	0.09
	Bottom	48.36	48.59			0.01	0.22		
B3	Top	32.817	32.69	78.92	78.84	-0.23	-0.22	0.04	0.08
	Bottom	46.10	46.15			0.28	0.30		
B4	Top	46.558	46.56	78.92	78.92	0.25	0.23	0.13	0.23
	Bottom	32.36	32.36			-0.12	0.00		
B5	Top	47.83	48.21	78.51	78.61	0.30	0.32	0.24	0.23
	Bottom	30.68	30.40			-0.07	-0.09		
B6	Top	48.18	47.90	78.84	78.79	0.45	0.43	0.11	0.10
	Bottom	30.66	30.89			-0.34	-0.33		
						Max	0.45	Max	0.24
						Min	-0.34	Min	-0.06
						Avg	0.06		
						Avg (abs)	0.20	Avg (abs)	0.07

TABLE B-2: A2 (Model 1) shim results

		Ordered, for Cbeam alignment				Case B Predicted			
A2		Shims sizes		Total gap size		Shims: Case B Predicted - Ordered		Gap: Case B Predicted - Ordered	
Bracket		Left (mm)	Right (mm)	Left (mm)	Right (mm)	Left (mm)	Right (mm)	Left (mm)	Right (mm)
B1	Top	48.77	48.46	79.15	79.07	-0.08	-0.07	0.09	0.11
	Bottom	30.38	30.61			0.17	0.18		
B2	Top	47.55	47.63	78.79	78.79	0.33	0.37	0.11	-0.24
	Bottom	31.24	31.17			-0.22	-0.61		
B3	Top	49.28	49.20	78.94	78.87	0.84	0.99	0.17	0.24
	Bottom	29.67	29.67			-0.67	-0.74		
B4	Top	30.43	30.61	79.15	78.92	0.44	0.48	0.21	0.25
	Bottom	48.72	48.31			-0.23	-0.22		
B5	Top	29.39	29.41	79.10	79.10	-0.06	0.04	0.10	0.09
	Bottom	49.71	49.68			0.16	0.05		
B6	Top	27.36	27.53	78.99	79.10	-0.56	-0.52	0.09	-0.50
	Bottom	51.64	51.56			0.66	0.02		
						Max	0.99	Max	0.25
						Min	-0.74	Min	-0.50
						Avg	0.03		
						Avg (abs)	0.36	Avg (abs)	0.09

TABLE B-3: A3 (Model 1) shim results

A3		Ordered, for Cbeam alignment				Case B Predicted			
		Shims sizes		Total gap size		Shims: Case B Predicted - Ordered		Gap: Case B Predicted - Ordered	
Bracket		Left (mm)	Right (mm)	Left (mm)	Right (mm)	Left (mm)	Right (mm)	Left (mm)	Right (mm)
B1	Top	37.67	37.31	78.59	78.66	-0.14	-0.10	0.10	0.08
	Bottom	40.92	41.35			0.25	0.18		
B2	Top	36.35	36.45	78.69	78.71	0.17	0.22	0.06	0.03
	Bottom	42.34	42.27			-0.11	-0.19		
B3	Top	38.99	38.25	78.69	78.66	0.70	0.77	-0.03	0.01
	Bottom	39.70	40.41			-0.74	-0.76		
B4	Top	42.32	42.42	78.74	78.74	-0.56	-0.56	0.07	0.01
	Bottom	36.42	36.32			0.63	0.58		
B5	Top	41.05	41.35	78.77	78.74	-1.12	-1.05	-0.03	-0.01
	Bottom	37.72	37.39			1.09	1.04		
B6	Top	40.46	40.82	78.71	78.71	-1.10	-1.08	0.05	0.05
	Bottom	38.25	37.90			1.15	1.13		
						Max	1.15	Max	0.10
						Min	-1.12	Min	-0.03
						Avg	0.02		
						Avg (abs)	0.64	Avg (abs)	0.02

TABLE B-4: A4 (Model 1) shim results

A4		Ordered, for Cbeam alignment				Case B Predicted			
		Shims sizes		Total gap size		Shims: Case B Predicted - Ordered		Gap: Case B Predicted - Ordered	
Bracket		Left (mm)	Right (mm)	Left (mm)	Right (mm)	Left (mm)	Right (mm)	Left (mm)	Right (mm)
B1	Top	76.10	75.82	154.89	154.84	0.69	0.73	0.12	0.11
	Bottom	78.79	79.02			-0.57	-0.62		
B2	Top	76.35	76.15	154.71	154.71	0.96	1.09	0.11	0.17
	Bottom	78.36	78.56			-0.84	-0.92		
B3	Top	76.25	76.56	154.89	154.91	1.20	1.21	0.15	0.11
	Bottom	78.64	78.36			-1.05	-1.10		
B4	Top	77.98	78.11	154.82	154.81	-0.09	-0.11	0.21	0.15
	Bottom	76.84	76.71			0.30	0.25		
B5	Top	77.80	77.72	154.79	154.76	-0.13	-0.12	0.11	0.07
	Bottom	76.99	77.04			0.24	0.19		
B6	Top	78.74	78.23	154.81	154.81	-0.06	-0.07	0.22	-0.12
	Bottom	76.07	76.58			0.28	-0.04		
						Max	1.21	Max	0.22
						Min	-1.10	Min	-0.12
						Avg	0.06		
						Avg (abs)	0.54	Avg (abs)	0.07

TABLE B-5: A5 (Model 2) shim results

A5		Ordered, for Cbeam alignment				Case B Predicted			
		Shims sizes		Total gap size		Shims: Case B Predicted - Ordered		Gap: Case B Predicted - Ordered	
Bracket		Left (mm)	Right (mm)	Left (mm)	Right (mm)	Left (mm)	Right (mm)	Left (mm)	Right (mm)
B1	Top	36.50	36.60	79.60	79.60	0.52	0.49	0.11	0.17
	Bottom	43.10	43.00			-0.42	-0.32		
B2	Top	34.80	35.10	79.60	79.70	0.43	0.48	0.14	-0.12
	Bottom	44.80	44.60			-0.29	-0.60		
B3	Top	35.30	35.60	79.80	79.80	0.40	0.46	0.10	0.05
	Bottom	44.50	44.20			-0.30	-0.41		
B4	Top	43.00	42.80	79.80	79.80	-0.22	-0.27	-0.15	-0.12
	Bottom	36.80	37.00			0.08	0.15		
B5	Top	42.20	41.60	79.60	79.60	0.01	-0.10	0.14	-0.30
	Bottom	37.40	38.00			0.13	-0.20		
B6	Top	43.70	43.00	79.60	79.90	-0.02	-0.25	-0.03	-0.34
	Bottom	35.90	36.90			-0.01	-0.09		
						Max	0.52	Max	0.17
						Min	-0.60	Min	-0.34
						Avg	-0.01		
						Avg (abs)	0.28	Avg (abs)	0.07

TABLE B-6: A6 (Model 2) shim results

A6		Ordered, for Cbeam alignment				Case B Predicted			
		Shims sizes		Total gap size		Shims: Case B Predicted - Ordered		Gap: Case B Predicted - Ordered	
Bracket		Left (mm)	Right (mm)	Left (mm)	Right (mm)	Left (mm)	Right (mm)	Left (mm)	Right (mm)
B1	Top	36.55	36.57	79.81	79.88	-0.29	-0.25	-0.08	-0.05
	Bottom	43.26	43.31			0.21	0.20		
B2	Top	36.07	35.94	79.83	79.80	-0.42	-0.35	-0.10	0.15
	Bottom	43.76	43.86			0.31	0.49		
B3	Top	35.69	35.56	79.81	79.88	-0.55	-0.60	0.11	-0.04
	Bottom	44.12	44.32			0.65	0.55		
B4	Top	41.78	41.53	79.85	79.88	0.30	0.31	0.10	0.08
	Bottom	38.07	38.35			-0.21	-0.24		
B5	Top	42.36	42.36	79.77	79.77	0.20	0.24	0.08	0.18
	Bottom	37.41	37.41			-0.12	-0.06		
B6	Top	42.21	42.16	79.70	79.65	-0.06	0.17	0.09	0.20
	Bottom	37.49	37.49			0.14	0.03		
						Max	0.65	Max	0.20
						Min	-0.60	Min	-0.10
						Avg	0.03		
						Avg (abs)	0.29	Avg (abs)	0.05

APPENDIX C. REFERENCE POINT DISPLACEMENT

TABLE C-1: RPD for several of the proposed process Frame and Core measurements

Generator	Support condition	Instrument Position	Max (mm)	RMS (mm)	Cause
A1 Frame	Ribs on wood	NLE	0.025	0.088	
		LE	0.212	0.159	Unknown
A3 Frame	Parallels	NLE	0.123	0.099	
		LE	0.050	0.038	
A4 Core	v-blocks	LE North brackets	0.212	0.159	Rail road car moved during measurement
		LE North brackets redo	0.074	0.040	
		LE center	0.070	0.040	
		LE South brackets	0.094	0.056	
A4 Frame	Ribs on plastic	NLE	0.169	0.116	
		LE	1.672	1.224	Foot of tracker was on groove in concrete
		LE redo	0.207	0.146	Unknown
A5 Core	v-blocks	LE North brackets	0.080	0.045	
		LE center	0.070	0.047	
		LE South brackets	0.057	0.038	
A5 Frame	Cbeam jacks	LE South	0.216	0.119	Unknown
		NLE	1.161	0.465	Neighboring generator was lifted
		LE North	0.123	0.062	
A6 Core	v-blocks	LE North brackets	0.097	0.056	
		LE center	0.068	0.042	
		LE South brackets	0.260	0.154	Meeting caused 1 hour mid-measurement delay
A6 Frame	Ribs on plastic	NLE	0.385	0.320	Unknown
		LE	0.117	0.082	